

## MAGNETOSHEATH INTERACTION WITH HIGH LATITUDE MAGNETOPAUSE

S. Savin<sup>1</sup>, P. Song<sup>3</sup>, A. Skalsky<sup>1</sup>, L. Zeleny<sup>1</sup>, E. Amata<sup>6</sup>, J. Buechner<sup>7</sup>, J. Blecki<sup>9</sup>, L. Avakov<sup>1</sup>, N. Borodkova<sup>1</sup>, G. Consolini<sup>6</sup>, C. Farrugia<sup>15</sup>, T.A. Fritz<sup>14</sup>, H. Kawano<sup>4</sup>, S. Klimov<sup>1</sup>, V. Lutsenko<sup>1</sup>, N. Maynard<sup>2</sup>, Z. Nemecek<sup>8</sup>, B. Nikutowski<sup>7</sup>, E. Panov<sup>1</sup>, J. Pickett<sup>10</sup>, M. Parrot<sup>11</sup>, J.L. Rauch<sup>11</sup>, S. Romanov<sup>1</sup>, C. T. Russell<sup>5</sup>, J. Safrankova<sup>8</sup>, I. Sandahl<sup>13</sup>, J.A. Sauvaud<sup>16</sup>, V. Smirnov<sup>1</sup>, K. Stasiewicz<sup>12</sup>, J.G. Trotignon<sup>11</sup>, Yu. Yermolaev<sup>1</sup>

<sup>1</sup> Space Research Institute, Profsoyuznaya 84/32, Moscow, 117810, Russia, <sup>2</sup> Mission Res. Corp, Nashua, NH, USA, <sup>3</sup> University of Massachusetts at Lowell, Lowell, MA, USA, <sup>4</sup> Kyushu U., Japan, <sup>5</sup> IGPP, UCLA, Los Angeles, CA, USA, <sup>6</sup> Interplanetary Space Phys. Inst., CNR, Roma, Italy, <sup>7</sup> Max-Planck Inst. Aeronomie, Katlenburg-Lindau, Germany, <sup>8</sup> Faculty Math. Phys., Charles U., Praha, Czech Republic, <sup>9</sup> Space Res. Center, Polish Academy Sci., Warsaw, Poland, <sup>10</sup> U. Iowa, USA, <sup>11</sup> Laboratory Phys. & Chemistry Environment, Orleans, France, <sup>12</sup> IRF-U, Uppsala, Sweden, <sup>13</sup> Inst. Space Physics, Kiruna, Sweden, <sup>14</sup> Boston U., USA, <sup>15</sup> U. N. Hampshire, USA, <sup>16</sup> CESR, Toulouse, France,

### ABSTRACT

*We present both statistical and two case studies of magnetosheath (MSH) interaction with the high latitude magnetopause (MP) on the basis of Interball-1 and other ISTP spacecraft data. The results of our data analysis strongly indicate that the TBL fluctuations, instead of being random, are phase-coupled and ‘organized’ by the cascades of nonlinear, presumably 3-wave, interactions. The selected coherent wave trains are capable of synchronizing interactions throughout the TBL, somewhat resembling a global TBL resonance. Multiplying the characteristic period of the ‘organizing’ wave mode by the MSH Alfvén speed we get 3-4 Re as a proxy for the characteristic scale. This is close to the diameter of the TBL or outer cusp throat and can be attributed to a standing nonlinear wave, trapped in the outer cusp throat. The quasi-coherent structures control the spectral shape and result in non-Gaussian statistical characteristics of the disturbances, that conforms the fluctuation intermittency. We suggest that multi-scale TBL processes play at least a comparable role to those of reconnection remote from the cusp in the solar wind energy transformation and population of the magnetosphere by the MSH plasma. The TBL transforms the MSH flow energy including deceleration and heating of the flow downstream the high latitude cusp. The plasma-plasma interaction over cusp throat operates via reflected waves, which ignite the chaotization of ~ 40% upstream kinetic energy, the sub-Alfvénic flow decay launches the TBL nonlinear cascades along with the jets accelerated downstream up to 3 Alfvénic Mach numbers*

### 1 INTRODUCTION.

Early single spacecraft observations with Heos-2 and later Prognoz-7, 8, 10 have shown that the magnetopause (MP) position and magnetosheath plasma flow structures are quite variable near the cusp, a magnetospheric region that is crucial for magnetosheath plasma entry (Paschmann et al., 1976; Haerendel and Paschmann, 1975; Klimov et al., 1986, Lundin et al., 1991; Savin, 1994). Haerendel (1978) was the first to introduce the turbulent boundary layer (TBL) in cusp physics in a discussion on the interaction of the magnetosheath flow with the magnetopause at the flank of the tail lobe. We reproduce his TBL sketch in Figure 1 (left panel): a laminar hydrodynamic flow interacts with an obstacle by generation of TBL both in front of the obstacle (marked by “1”) and behind it (marked by “2”). The zone “1” corresponds to the funnel-shaped cusp throat in the right sketch of Figure 1, the obstacle is presented by uprising magnetic field tubes at the tailward cusp

wall. The downstream zone “2” has been poorly studied (see Savin et al., 2002a and references therein), it represent an aim for this paper.

Because of differences in the data, researchers have divided the high altitude cusp into a number of layers and regions. Since full agreement on how this should be done is not yet achieved, we will give the definitions and descriptions of the regions discussed in this paper. These regions, shown in right panel of Figure 1, are: the outer and inner cusps, the outer cusp throat (OT) and the turbulent boundary layer. We will demonstrate however, that the interaction pattern in Figure 1 should be modified for winter cusp crossings. The reader is referred to the papers by Smith and Lockwood (1996) and Angelopoulos et al., (2001) for a synopsis of measurements and models of the low altitude cusp.

Referring to Figure 1, the outer cusp throat (slant-line shaded region) is outside the MP, the outer cusp (gray) is just inside the MP, and the inner cusp (black) is deeper in the magnetosphere. We identify here the MP (inner white line) as the innermost current sheet where the magnetic field turns from Earth-controlled to magnetosheath-controlled (Haerendel and Paschmann, 1975). The outer cusp is a region with three different particle populations: newly injected MSH ions, MSH ions reflected from the ionosphere, and quasi-perpendicular ions trapped in the local magnetic field minimum near the cusp (Savin et al., 1998b, Sandahl et al., 2000). There are also electrons accelerated along the field lines. The newly injected and quasi-perpendicular ions dominate over those that are reflected. This is one of the characteristics distinguishing the outer cusp from the inner cusp and from the distant mantle. The outer cusp is also characterized by moderate magnetic noise while in the inner cusp there is a similar type of noise observed primarily only at the boundaries (Pottelette et al., 1990). The outer cusp consists of the entry layer and the portion of the plasma mantle adjoining the entry layer (Paschmann et al., 1976). According to the work of Yamauchi and Lundin (1997) the entry layer and mantle that are parts of the outer cusp form one continuous region. At the cusp the magnetopause is indented. This indentation was first predicted by Spreiter and Briggs (1962) and then detected by HEOS-2 (Paschmann et al., 1976), ISEE (Petrinec and Russell, 1995), and Hawkeye-1 (Chen et al., 1997). Zhou and Russell (1997) found that the MP is closer to the Earth at high latitudes than at low latitudes. Interball-1 early statistics show that the indentation is on the average about 2  $R_E$  deep (Savin et al., 1998b). We call this part of the exterior cusp the outer cusp throat. The plasma in the outer cusp throat is highly disturbed and/or stagnant MSH plasma. The difference between our outer cusp throat and the "stagnation region" defined by Haerendel et al. (1978) is that the stagnation region has no specific relation to the magnetopause, as noted by the multiple arrows in Plate A1. Usually, the magnetopause can be recognized in both Polar and Interball-1 data, but when this is not the case it is better to use the term "stagnation region", rather than "outer cusp throat".

The turbulent boundary layer is a region dominated by irregular magnetic fields and plasma flows. It is located just outside and/or at the near cusp magnetopause and has recently been found to be a permanent feature (Savin et al., 1997, 1998b, 2002, Klimov et al., 1997, Sandahl et al., 2000). Here the energy density of the ultra low frequency (ULF) fluctuations is comparable to the ion kinetic, thermal, and DC magnetic field densities. The ULF power is usually several times larger than that in the MSH, and one or two orders of magnitude larger than that inside the magnetopause. As recent studies conclude (see e.g. Belmont and Rezeau, 2001 and references therein) the strong ULF fluctuations that occur just outside of or at the magnetopause can independently result in micro-reconnection and local plasma penetration all along the magnetopause surface even without the presence of quasi-stationary global reconnection. In two case studies Savin et al. (1998b) have shown that large-scale structures ( $> 30$  s) tend to be spatial, while for shorter time scales the temporal changes are significant. We utilize the magnetic AC power related to the average plasma and field energy density in the magnetosheath as a rough measure of the strong turbulence regime. This ratio being  $> 0.1$  corresponds to strong diffusion discussed in the percolation theory of Kuznetsova & Zelenyi (1990). Examples of highly turbulent magnetic and electric fields in the exterior cusp have been reported by Paschmann et al. (1976) and Haerendel et al. (1978) from Heos-

2, by Klimov et al. (1986) from Prognoz-10, by Savin (1994) and Blecki et al. (1998), from Prognoz-8 and by Chen et al. (1997) from Hawkeye-1 data. Prognoz-8 and 10 magnetic field experiments had high enough sampling rate (1-50 Hz versus  $\sim 0.03$  Hz on Heos-2 and Hawkeye-1) for turbulent boundary layer studies. However, the absence of 3D plasma measurements and poor statistics prevented a systematic study of the turbulent boundary layer signatures and of the TBL's role in mass and momentum transport at the high latitude magnetopause.

The main goal of this paper is to survey the achievements and explore solutions to the problems associated with the TBL and exterior cusp physics in the Interball era. The recent baseline case studies are described in details in Savin et al., (2001, 2002a, 2002b, 2003a and 2003b). We present for the first time full statistical review of the high level ULF magnetic turbulence (i.e. of the TBL) from the Interball-1 data, concentrating on the MP asymmetry for the summer and winter hemispheres. The permanent plasma heating in TBL is regarded as a result of transformation of the MSH flow energy into the random and thermal ones in the process of the MSH flow interaction with the outer cusp throat. Two cases are utilized to display the characteristic TBL features.

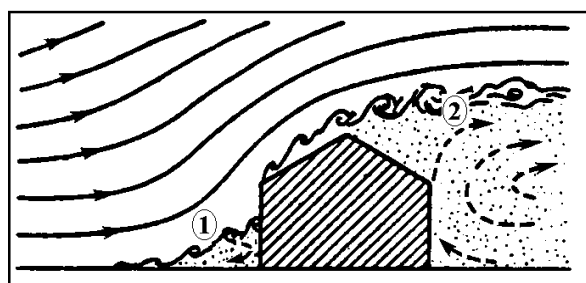
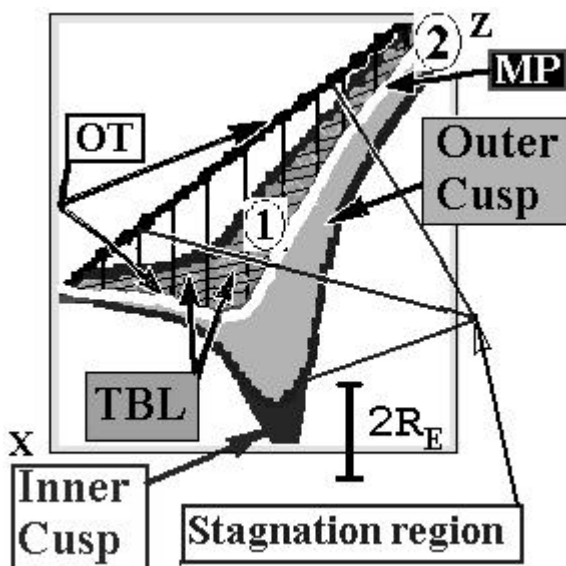


*Fig.1. Top: Generation of turbulent boundary layer in the process of interaction of hydrodynamic flow with obstacle (from Haerendel, 1978). "1" – marks open cusp throat, "2" – stands for high latitude boundary layer downstream the cusp.*

*Right: Sketch for MSH/cusp interface in noon-midnight plane from (Savin et al., 2002a). The boundaries and sub-regions are described in text.*



We discuss data from Interball-1,2, Magion-4 (Interball-1 sub-satellite), Geotail and Polar on January 27, 1997 over a winter cusp and compare them with results of Spreiter model of the solar wind (SW) interaction with the magnetosphere. The main question we address here is whether the turbulent boundary layer and the outer cusp throat play a substantial role in the magnetosheath plasma flow interaction with the high latitude MP. The multi-point data provide evidences that downstream the cusp the MSH flow is decelerated and heated as compared with the near-equatorial MSH flow. While being permanent, the ion heating in TBL is too weak to account for the ion energies in the lower altitude boundary cusp and 'sash', detected by Interball-2 and Polar respectively.

Another example of the winter TBL encounter by Interball-1 on June 19, 1998 serves to demonstrate the asymmetry of boundary layers for positive (sunward) Earth magnetic dipole tilts in summer and that of the negative (anti-sunward) tilts in winter. The difference has been established by Savin et al. (2002a) by comparison with simultaneous Polar data in the summer stagnation region. We reproduce most interesting results from the previous studies (cf. Savin et al., 2003b) and analyze detailed dynamics of the ion energy and of Poynting flux to clarify the pattern of nonlinear interactions in the upstream TBL. The wave packets, going upstream MSH flow from MP, occur to stimulate partial

randomization of the flow far in front of MP, the SW driving plays the minor role. The interaction with the upstream waves launches downstream current sheets, which confine super-Alfvénic tailward jets. That signifies the cascade-like non-linear energy transformation in TBL, proposed by Savin et al. (2001). We exhibit de-magnetized large-scale ‘plasma balls’ inside winter MP and study their statistics versus that of heated MSH plasma outside MP in summer.

Finally, we discuss the presented and published Interball-1 data in relation to the MSH plasma penetration and acceleration both due to plasma percolation and turbulent heating and due to laminar large-scale reconnection of anti-parallel magnetic fields.

## 2 MAGNETOSHEATH- MAGNETOPAUSE INTERACTIONS ON JANUARY 27, 1996.

We would like to start from an example of the TBL encounter on January 27, 1997 by Interball-1 and Magion-4, which started over northern cusp (tilt  $\sim -21$  degrees, i.e. winter period) and proceeded in the near tail in so called ‘sash’ (Maynard et al., 2001). The respective substorm-related features are discussed in Savin et al. (1998c). Here we are concentrating on the boundary layer behavior. Comparison with simultaneous Geotail, Interball-2, Polar and WIND SW data provides the opportunity to distill the influence of the TBL-related effects on the penetrating MSH plasma and on the MSH flow downstream the cusp.

In Figure 2 we present the Tsyganenko-96 model magnetic field lines and positions in GSM coordinates of different spacecraft by circled ‘I’, ‘M’, ‘P’, ‘A’ and ‘G’ for Interball-1, Magion-4, Polar, Interball-2 and Geotail, respectively on January 27, 1997. Magion-4 was about 2 Re deeper into magnetosphere than

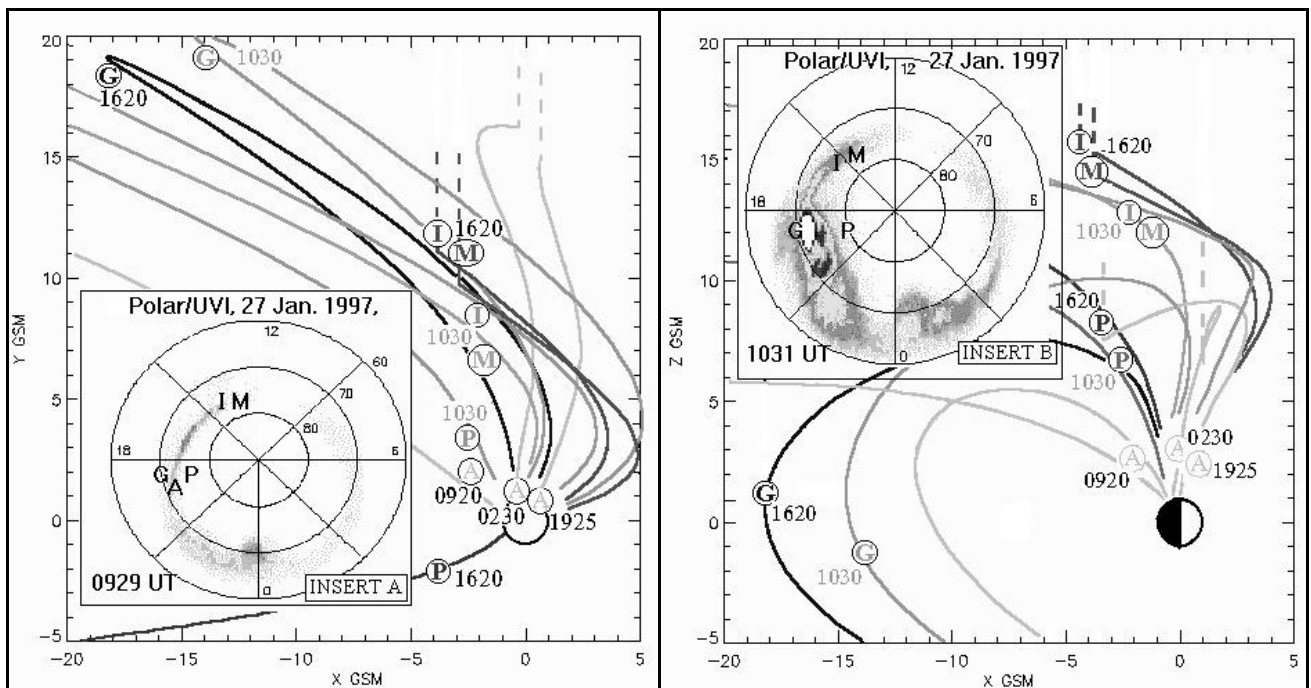


**Fig. 2.** Positions of the spacecraft in GSM XZ (right) and XY (left) planes and Tsyganenko-96 magnetic field lines on January 27, 1997 (see text for details). ‘I’ marks – Interball-1, ‘M’ – Magion-4, ‘G’ – Geotail, ‘P’ – Polar, ‘A’ – Interball-2; UT is displayed near spacecraft positions. Dashed field lines are outside MP without taking into account IMF Bx. INSERTS A and B display spacecraft footprints onto northern ionosphere at 0929 and 1031 UT, UVI Polar camera images are superimposed.

Interball-1 along the average MP normal (and  $\sim 3$  Re apart along the orbit). Note that generally all spacecraft were in the dusk magnetosphere (except Polar at 16:20 UT), Interball-1 crossed high latitude

MP, Geotail was near equator just inside MP and Interball-2 monitored lower altitude boundary cusp. The ultra-violet (UVI) Polar camera data (Inserts A & B) infers that, while being far away from the rest spacecraft, Interball/Magion pair monitors the same day-side MSH plasma penetration (at ~ 09:30-10:30 UT) from its different edges. At 10:31 UT Geotail leaved magnetosphere for the short time in result of substorm activities (Savin et al., 1998c), the substorm effect is seen in brightening of the aurora in Insert B close to the Geotail footprint (marked by "G").

In Figure 3 we present combined Geotail, Interball-1, Polar/TIMAS and WIND SW data (the latter shifted by approximate SW propagation time lag of 42 minutes, panel a). The GSM Bz- component is gray-shadowed, the dynamic pressure P<sub>dyn</sub> is depicted by dashed line. Panels b (magnetospheric encounters are gray shadowed) and c give different components of the energy density (for Geotail and Interball-1 respectively), the thermal energy density (dashed line),  $E_t = 1.5 n k T_i$  (where n - plasma density,  $T_i$  - ion temperature), the kinetic energy density,  $E_k = 0.5 n M_i V_i^2$  (where  $M_i$  and  $V_i$  - ion mass and velocity) and the magnetic energy density,  $E_m = |B|^2/8\pi$  (gray shadowed); panel d: ion temperature  $T_i$  with black shadowed heating; panels e and f (for Interball-1 and Geotail): the power contained in the magnetic field variations –  $D_f$  in the range 0.0085-2 Hz, and the gray-shadowed variation of magnetic field magnitude  $D_m$  ( $D_f$  is obtained by taking the sum of variation powers in B<sub>x</sub>, B<sub>y</sub> and B<sub>z</sub> and then using the relation 1 eV ~ 2.49 nT<sup>2</sup> to express  $D_f$  in energy density units); panels g and h: tailward ion flow from Faraday cups (on Interball-1 and Magion-4, respectively) in arbitrary units, magnetospheric encounters are gray shadowed (cf. Savin et al., 1998c); panel i: Polar/TIMAS He<sup>++</sup> (shadowed) and low-energy proton (dashed line) densities and proton temperature. The temperature of Polar proton low-energy component is not shown inside empty polar cap. Interball-1 and Geotail positions in GSM frame are given at the bottom of Figure 3. This case represents an example of disturbed conditions (see frequent changes of WIND B<sub>z</sub> and B<sub>y</sub> signs). The Interball main outbound MP at ~ 10 UT is diffuse. The TBL threshold on panel e is chosen to be  $D_f > 36 \text{ nT}^2$  (black-shadowed, see also discussion in the next section), on panel f it is lower, that takes into account 4 Hz sampling for Interball data versus Geotail 0.33 Hz one.  $D_f$  on Geotail is lower even being related to the respective lower threshold. It indicates on the high latitude TBL as the possible source for the low latitude disturbances. These disturbances could be transferred along field lines from high latitudes (where they are much more powerful) towards low latitudes along field lines as Alfvén waves (cf. Savin et al., 1998c). Extra heating on Interball in TBL and OC is ~ in 1.5 times (black-shadowed on panel d in Figure 3). The OC is determined here from dominating of  $E_t$  over  $E_m$  (panel c) after 09:20 UT when  $E_k < E_m$ , MSH encounters are seen from the kinetic energy rises  $E_k > E_m$ . In the low latitude BL (Geotail) the  $T_i$  is close to the Interball value (see the  $T_i$  minima at 0930-1010, 1642-1650 UT and maxima at 1020, 1110, 1120 & 1700 UT on panel d in Figure 3). This is an indication on possible high latitude origin of the BL plasma.

The Interball/Magion data demonstrate that the most prominent disturbances are seen on both satellite and subsatellite as spiky flows on panels g, h. They correlate at 10:30-12:00 and 13:00-15:00 UT (excluding spin modulation and extra MP crossings by Magion-4, cf. upper gray-shadowing). For quieter periods in  $D_f$  on panel e at 10:15-10:30 & 12:30-13:00 UT the disturbances in the plasma flows are seen mostly in the Magion-4 data. Comparing the  $D_f$ ,  $E_m$  and the plasma flow data at 10-15 UT, we can do the order-of-magnitude estimate of the TBL depth in the tail 'wings' (see Plate 1A and respective discussion below) as being close to 2  $R_e$  (i.e. to the distance between spacecraft along the MP normal). It is supported by: (a) the correlation of the plasma flows is good for the major part of the TBL, i.e. spacecraft are mostly in the same region, nevertheless they leave it for short periods; (b) Magion-4 crosses MP much more often, the MP is believed to be close to the inner edge of TBL (i.e. Magion is close to the TBL bottom). This is the first direct probing of TBL depth in tail 'wings' and it is valuable that the depth has the same order of magnitude as the OT indentation and the 'core' TBL above the noon cusp (cf. Savin et al., 1998a).

The Interball-2 (Auroral) ion data from the spectrometer ION are shown in Figure 4 for the time intervals labeled in Figure 2 by letter "A" and UT times about 02:30 and 19:25 when the boundary cusp/cleft-like plasma has been seen. For both 02:30 and 19:25 UT T96 model shows the connection of the Interball-Auroral with MSH as well.

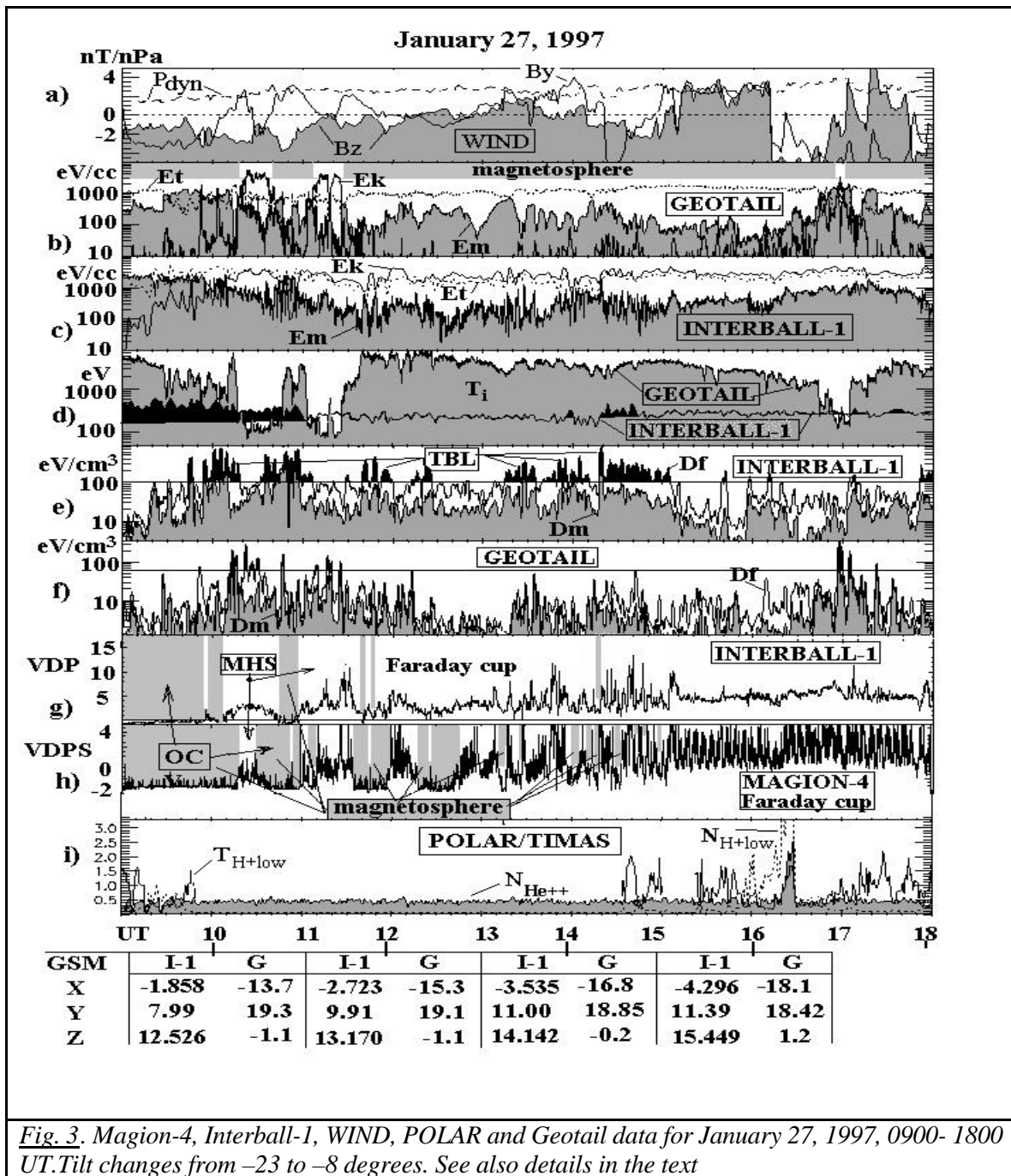


*Fig. 3. Magion-4, Interball-1, WIND, POLAR and Geotail data for January 27, 1997, 0900- 1800 UT. Tilt changes from  $-23$  to  $-8$  degrees. See also details in the text*

At 0915-0930 UT Interball-1 and Geotail encounter weak boundary layer (Figures 2, 3):

- on Geotail weak bursts of the MSH-like ions appear (not shown), thermal energy  $E_t$  dominates (panel b),  $T_i$  minima at about 0930 UT are of 600-800 eV;
- on Interball-1 density reaches 5 1/cc, ion kinetic energy density  $E_k$  changes from 70-100 to 400-800 eV/cc, ion thermal energy density become larger than the DC magnetic one (panel c), characteristic  $T_i = 500$  eV.

In the polar cap Polar registers low energy  $H^+$  ions (panel i) and ionospheric  $He^+$  and then  $O^+$  ions (not shown).

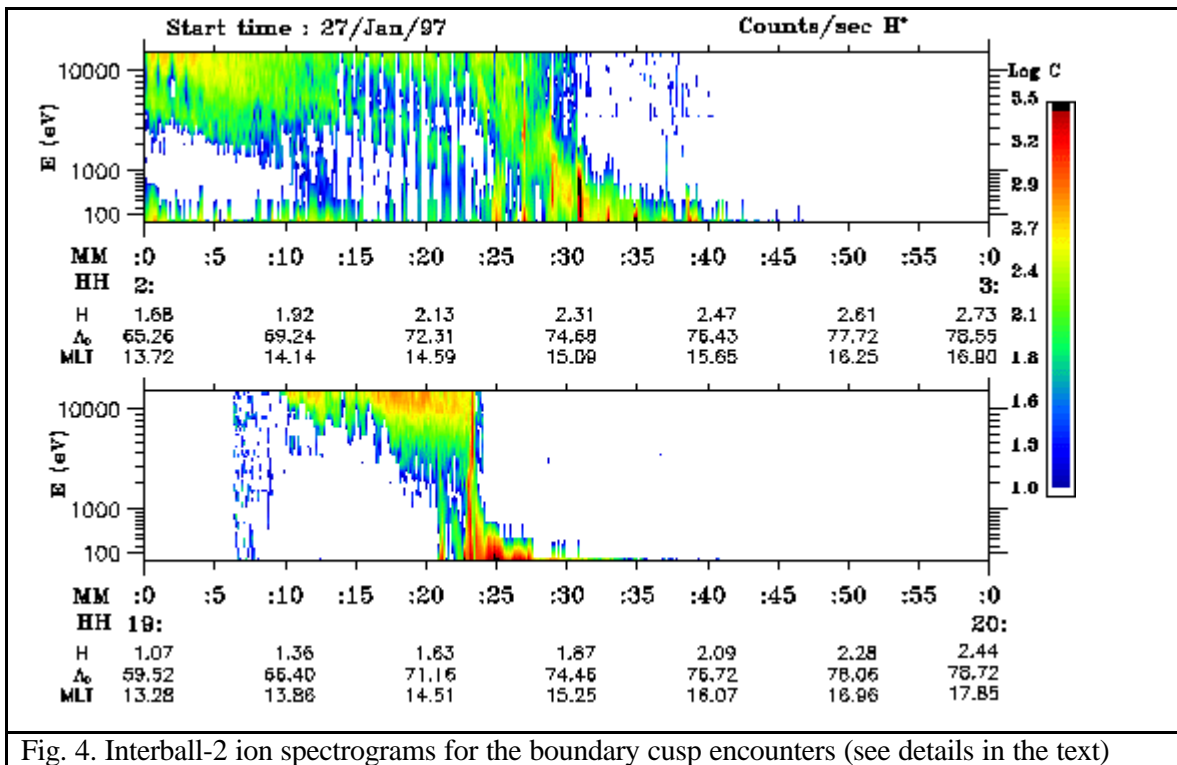


Fig. 4. Interball-2 ion spectrograms for the boundary cusp encounters (see details in the text)

IMF Bz (panel a in Figure 4, shadowed) is negative during Interball and Geotail weak BL encounter and MP crossings (since about 08 UT). Strong IMF By < 0 at the interval beginning (09 UT) shifts the northern reconnection site downward, the southern one - duskward i.e. towards Geotail (Maynard et al., 2001).

The positive By spike at about 10 UT would shift the northern reconnection site duskward (i.e. towards Interball-1 and Magion-4). It results in the Interball-1 transition from the cusp (before 09:30 UT) to BL/mantle (09:30-10:08 UT), in Figure 4 it could be seen from the ion kinetic energy density  $E_k$  being equal or higher than the energy of DC magnetic field  $E_m$  (panel c). At Geotail two "MSH injections" are seen at 09:43 and 09:54 UT as  $E_k$  spikes on panel b. The Interball-1 MP at 10:10 UT is diffuse and turbulent partially due to the IMF changes and partially due to the TBL crossings just outside MP, that coincides with velocity shear from the MP till 10:18 UT (see also Savin *et al.*, 1998c). In MSH (10:18-10:40 UT) on Interball-1  $E_k \sim E_t$ , that is in contrast to the Geotail situation where  $E_k \gg E_t$  in MSH. (panels b, c). Geotail outbound MP at 10:18 UT corresponds to the IMF By positive excursion (confirmed by Geotail By, not shown). At 10:30 – 15:00 UT the drops in the DC magnetic energy density  $E_m$  on Interball-1 (panel c) represent the 'diamagnetic bubbles' (see Savin et al. (1998a) and discussion in the next section). At 10 - 12 UT the 'magnetic bubbles' are seen in the Geotail  $E_m$  that coincides with the high-level Df zones. At 10:20-10:35 UT the Geotail Df resembles that of TBL on Interball-1 (panels e, f in Figure 3) by dominating of the non-compressible fluctuations (see big difference in the shadowed and full curves on panel f).

We propose that the difference in the  $E_k$ ,  $E_t$  and temperatures in MSH between Geotail and Interball-1 is mainly due to the high latitude TBL, where the part of the MSH flow kinetic energy  $E_k$  is transformed into the thermal one  $E_t$  as it has been proposed by Savin *et al.*, 1998b (see also discussion below). The effect might be seen near the tail MP even downstream the TBL as one can see from the Interball-1 data at 15:10-15:35 with very low Df, without 'diamagnetic bubbles' and with generally the same  $T_i$ . Extra ion heating is seen in the most intensive TBL-like sites on Interball-1, but it is much lower as compared with the difference between  $T_i$  and  $E_t$  on Geotail and

Interball-1 in MSH.  $E_k + E_t$  in MSH are nearly equal for both Interball-1 and Geotail (in about 20 %, on Interball-1 it is slightly higher), that is suggestive for compatibility of the ion measurements on the two spacecraft.

It's interesting, that there is no big difference between the ion characteristic energies on Interball-2 in the quasi-stationary situations at 02:30 and 19:25 UT (Figure 4) and the Polar ones during dynamic interaction of the magnetosphere with the SW discontinuity at 16:10 UT (Figure 3). The disturbance at 16-17 UT had the global character due to sharp change of the sign and magnitude of IMF  $B_y$  &  $B_z$ . The appearance of the disturbance in the dawn tail in the response to the negative  $B_y$  IMF turning corresponds to the 'sash' predictions (see e.g. Maynard et al., 2001). The Polar BL plasma identification deep in the polar cap is reliable due to  $He^{++}$  ions registration at about 16:25 UT (Figure 3, panel i, shadowed curve). Polar  $H^+$  temperature of 0.5-1.7 keV is not far from the ion characteristic energy at 02:30 and 19:25 UT on Interball-2 (Figure 4) in rather ordinary boundary cusps. It should imply that the mechanisms of the MSH ion acceleration in the boundary cusp/cleft for the stationary and in the 'sash' for dynamic cases are similar. The potential difference of few kV between the closed and open field lines might be the source of the acceleration (cf. Lundin *et al.*, 1991). On Interball-1 at the dusk MSH the discontinuity in IMF  $B_y$  and  $B_z$  is well seen, weak 'diamagnetic bubbles' preclude and accompany the discontinuity, the plasma flow disturbance is almost undetectable. In contrast to that, on Magion-4 the tailward flow is substantially decelerated (panels g, h in Figure 3), it tells that the dynamic disturbance have characteristic size of 1-2  $R_e$  outside MP. Somewhat later after 16:43 UT Geotail touched the tailward streaming BL and even MP (panel b in Figure 3) in the response on the IMF  $B_y$  becoming dominant negative; the latter would lead to the flank reconnection in the southern hemisphere below Geotail. Rather high Geotail  $D_f$  level (panel f in Figure 3) near MP at 16:58 UT coincide with the  $T_i$  rise till to the Interball-1 high latitude MSH level. It is an argument that Geotail was close to the reconnection site in which the incoming MSH plasma is heated similar to the high latitude TBL (cf. Savin *et al.*, 1997).

The multi-point data on January 27, 1997 provide an opportunity to get the quantitative estimate for the drop of the downstream kinetic energy density  $E_k$  (relative to the thermal one,  $E_t$ ) in the zone "2" in Figure 1 due to the MSH flow interactions with the tailward cusp wall. The model of Spreiter and Stahara (1980) predicts the gain of  $E_k/E_t$  to be  $\sim 2$  for Geotail relative to Interball-1 in Figure 2 of Savin et al. (1998c) at  $\sim 1120$  UT, while the measured gain is  $\sim 8$ , i.e.,  $E_k/E_t$  drops by a factor of  $\sim 4$  at high latitudes in comparison to the simultaneously obtained low latitude values at the same X. Following (Haerendel, 1978) we address this deceleration to the MSH flow interaction with rising field lines at the tailward wall of the outer cusp throat. The sound Mach number in the unperturbed MSH ( $M_s \sim 2.1$ ) drops to  $M_s < 1$  downstream of the cusp obstacle on April 21 1996 (Savin *et al.*, 1998b).  $M_s \sim 2$  is also seen in the Interball-1 data just outside the MP (Savin et al., 2003a), while the flow/discontinuity geometry in the cusp throat is not clear enough yet. The  $M_s$  supersonic/subsonic transitions are compatible with the existence of slow/intermediate shocks (see e.g. Russell 1995 and references therein) in the vicinity of the tailward cusp wall (cf. Yamauchi and Lundin, 1997 and Savin *et al.*, 1998b). Thus, we think that the finding of the MSH flow deceleration/heating downstream of the high latitude cusp represents a valuable result from the multi-spacecraft data that signifies the bulk flow energy transformation in the process of the flow interaction with the outer cusp throat.

### **3 TURBULENT BOUNDARY LAYER ENCOUNTERS BY INTERBALL-1 IN 1995- 2000 YEARS.**

After the presentation of a TBL encounter over the northern cusp and at the border of the near geomagnetic tail on January 27, 1997, we would like to overview the TBL mapping by Interball-1 in 1995- 2000 years. The Interball-1 orbit evolution provided opportunity to cross near-cusp MP along with the boundary between mantle and LLBL in the near tail twice per orbit (excluding late October - late December period). This orbit is the unique one for spacecraft with plasma and field experiments aboard.

For this study we use the routinely calculated dispersion of Bx row magnetic field waveform with sampling rate 4 Hz on the 2-minute intervals (i.e. for 0.0085-2 Hz). We multiply the Bx dispersion by factor 3 for comparison with Df in statistical sense (i.e. we suggest equality of the ULF average power for all 3 magnetic components). We give the AC magnetic pressure (= Df) in [eV/cc] for comparison with other energy densities. Similar to [Savin *et al.*, 2002a], we define the background TBL at a time interval of <20 minutes when B<sub>x</sub>-variation during 2-minute interval exceeds at least in two points threshold 3 nT (~5.2 nT for full variation or ~ 67 eV/cc), being in 1.5 times higher than that of nearby MSH. It is shown by gray-colored orbit pieces in Plates A1, A2 and A4. Note, that in previous TBL statistical studies (Savin *et al.*, 1999, 2002a, 2003a) the shorter time periods (1-3 years) and variation interval (20 seconds) have been used. We have checked for several characteristic TBL cases that the 2- minute variation interval is rather representative as Df starts to saturate with increase of the variation interval. For individual cases we choose the threshold as maximum out of the two values, 3 nT and 1.5 characteristic MSH Bx- variations (cf. threshold for Bx- variation ~ 3.7 nT (100 eV/cc) on panel e in Figure 3). We have found 651 TBL events for about 400 MP crossings, thus most MP crossings bear multiple TBL encounters according to the definition above.

In Plate A1 we display in 3 GSM planes the color-coded distribution of the events with high magnetic variance as function of the Bx-variation magnitude (D(Bx)), the colors for respective variation intervals are depicted in the left lower corner. We limit our study outward the magnetosphere by minimum of two values: (a) half a distance between most distant from the Earth MP and closest to the Earth bow shock (BS) at the same orbit, (b) 5 Re outward from the most distant MP. We exclude single spikes in Bx- variation clearly corresponded to the main magnetic field changes at MP itself. The gray-colored TBL background serves mostly to mark the near-MP coverage by the Interball-1 orbits. Note the gap for  $Z < -14$  Re and  $|X|, |Y| < 7$  Re (which is due to the Interball-1 re-enter in October 2000). The tail MP around midnight is not covered by Interball-1 (blank area in the center of XY- plane at negative X), while the dayside one is.

In Plate A1 events concentrate at high latitudes ( $|Z| > 4$  Re) near OT and downstream it, especially it is well seen for variations  $> 8$  nT (blue and red colors). Namely those events are associated with TBL per se. On YZ- plane at low latitudes one can also recognize groups of intensive events (for both positive and negative Y), XZ- plane demonstrates that most of them are encountered in the tail. The latter corresponds to the 'sash' predictions (Maynard *et al.*, 2001). The northern (upper) TBL is indented in the YZ- plane, that corresponds to the MP indentation (cf. Savin *et al.*, 1998a and Figure 1). In the southern hemisphere no indentation can be inferred. To prove that it is not an effect of the coverage absence at the large negative Z, let's compare the event appearance along directions  $Z = 10$  Re and  $Z = -10$  Re: in the former case there is clear maximum in vicinity of  $Y \sim 0$ , while in the latter case there is minimum in the event occurrence (shifted to the positive Y). The mentioned above peculiarities are even better seen in Plate A2, where the gray-scaled background events are given in the same format, while the rest color-coded ones are shown only for Bx- variations  $> 8$  nT (see discussion of the tilt dependence below).

In Plates A1 and A2 we would like to outline also the TBL 'wings' on planes XY and XZ, ranging from the near-cusp TBL into the tail down to  $X \sim -20$  Re. Interball-1/Magion-4 orbit on January 27, 1997 (Figures 2 and 3) is in the middle of a 'wing'. Savin *et al.* (2002a) have demonstrated that a substantial part of the events in those 'wings' at the higher latitudes is independent on the interplanetary (IMF) B<sub>y</sub>, which contradicts the 'sash' predictions. Approximately another half of the 'wing' events follows the 'sash' B<sub>y</sub>-dependence (cf. the mentioned above low-latitude events). The higher-latitude 'wings' are in vicinity of the boundary between semi-open mantle lines and closed LLBL lines, the local minimum in the total magnetic field and currents providing field rotation from the open to closed lines are anticipated there. Another possible 'wing' source is the downstream TBL, discussed in the previous section (see Figures 1, 3 and related discussions).

The presence of TBL 'wings' for any IMF B<sub>y</sub> could conform the MSH plasma penetration not only in the

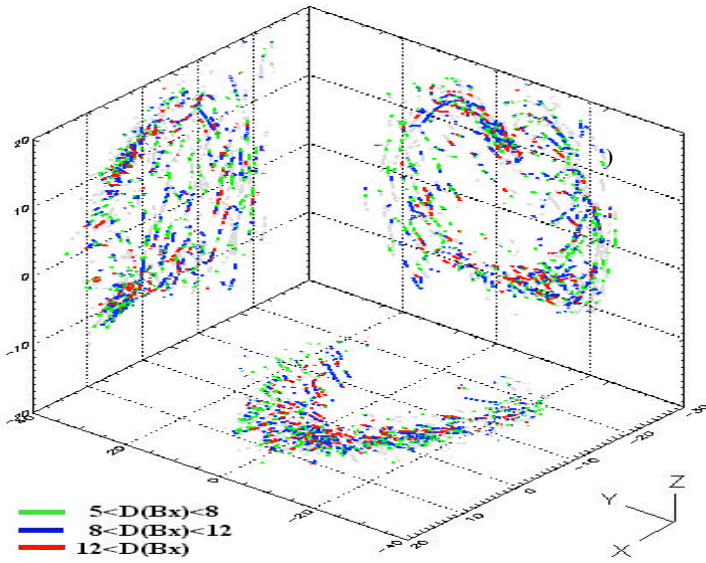


**Plate A1.** TBL level map (nT) in 3 GSM planes (gray color -  $D(B_x) > 3nT$ )

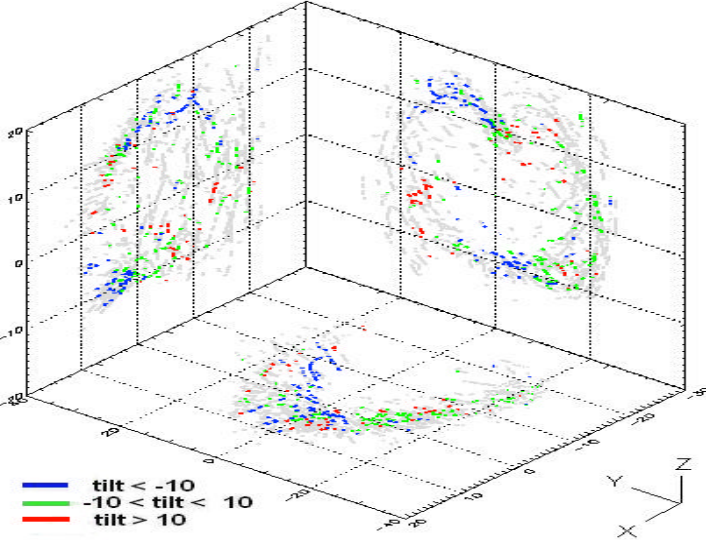


**Plate A2.** TBL tilt dependence for  $D(B_x) > 8nT$

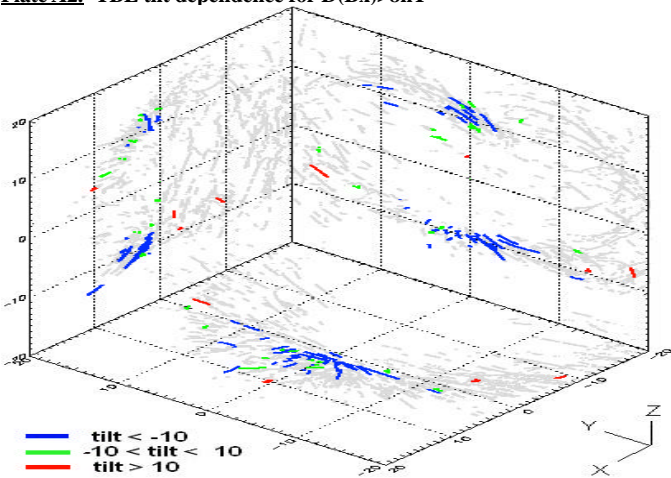


**Plate A3.** PB tilt (degrees) dependence (gray color - TBL)

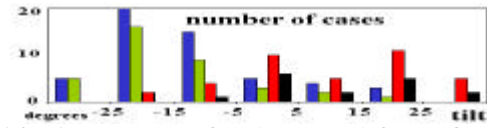


**Plate A4.** Tilt dependence of PB (blue, green) & open OT

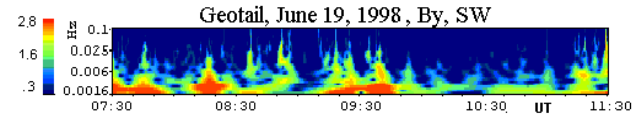


**Plate A5.** SW By spectrogram (Geotail) on June 19, 1998

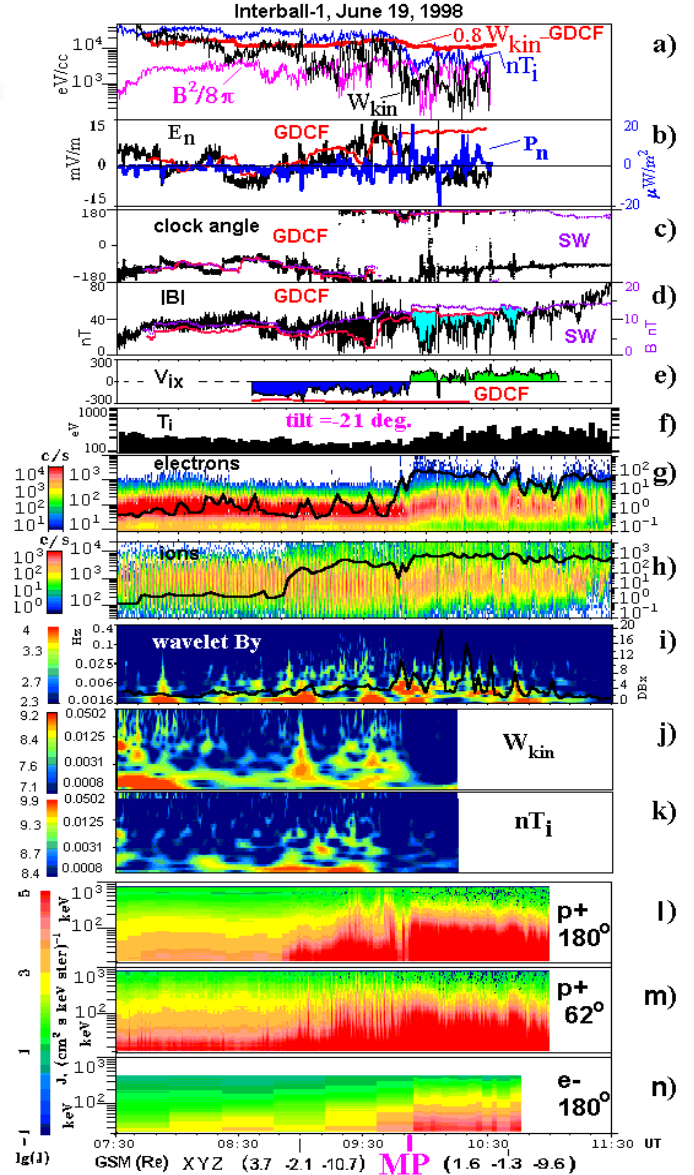


**Plate A6.** TBL and PB on June 19, 1998. (a) energy densities; (b) normal electric field and Poynting vector; (c) magnetic clock angle; (d)  $|B|$ ; (e) ion Vx velocity; (f) ion temperature; (g) electron spectrogram & intensity ( $>30$  keV); (h) ion spectrogram & intensity ( $>30$  keV); (i) magnetic By- spectrogram & Bx-variation; (j) ion kinetic energy spectrogram; (k) ion thermal energy spectrogram; (l-n) energetic ions (FOV 180 & 62 deg. from Sun) & electrons (FOV 180 deg. from Sun)

cusplike dayside and 'sash' regions, but on the tail flanks per se (cf. Haerendel *et al.*, 1978). This is valid in both cases: if turbulent diffusion provides the necessary mass transport by itself and/or if the turbulence serves as the indicator of local reconnections. Note, that although Klimov *et al.* (1997) and Savin *et al.* (1997) already reported the TBL-like signatures in the tail, the problem of the TBL sources in the tail is still far from completion.

Figure 3 demonstrates that in TBL the compressible magnetic field disturbances are also present. While they are not dominant in the TBL power, the spiky magnetic field drops – 'diamagnetic bubbles' (DB, see Savin *et al.*, 1998a) – provide a mechanism for the plasma heating in TBL. For the statistics of the 'diamagnetic bubbles' Savin *et al.* (1999) used maximum depths of the spiky total field (Bt) drops to calculate the diamagnetic effect of the heated MSH plasma inside the 'diamagnetic bubbles'. The 'bubble's' distribution (not shown, see e.g. Romanov *et al.*, 1999) is generally the same as the TBL event ones in Plates A1 and A2. The averaged maximum plasma pressure excess in 'magnetic bubbles' is  $d(NT) = 2160$  eV/cc. The magnetic field inside the 'bubble' is in 8,3 times weaker than outside. Taking plasma density in TBL of 5-10 1/cc, one gets the plasma heating on 216-430 eV inside the 'magnetic bubbles', i.e. heating in 1.5-3 times relative to the temperature of the MSH ions. This is in good correspondence with predictions of Haerendel (1978). The most events with  $Df > (15 \text{ nT})^2$  and  $d(NT) > 3100$  eV/cc are seen at  $|Z| > 4 \text{ Re}$ , their maximum above the cusp is most prominent. Intensive heating in the high latitude tail 'wings' is seen only till  $X = -6 \text{ Re}$ .

Merka *et al.* (1999) had shown, that the most prominent dependence for the exterior cusp is the dependence from the dipole tilt angle. Their study has been restricted by the northern hemisphere, in which for the majority of MP encounters by Interball-1/ Magion-4 the tilt was positive. Their definition of the exterior cusp includes TBL as a part (see Figure 1 and related discussion above).

As we have discussed above, XY- plane in Plate A1 infers asymmetry between northern (mainly summer for Interball-1) and southern (winter) hemispheres even in the shape of TBL. Thus we would like to look for the tilt dependence of the TBL-like events. In Plate A2 we present the map of TBL events, color-coded by the magnetic dipole tilt angle (see the colors and corresponding tilt ranges in the left bottom corner). The format is the same as for Plate A1, including gray-colored background TBL events with the lowest threshold. For the analysis we have chosen only strong TBL-like events with the  $B_x$ - variation  $> 8 \text{ nT}$  (480 eV/cc). In the northern indentation the events with positive and zero tilts dominate. It conforms direct interactions of the open cusp throat with the incident MSH flows (marked "1" in Figure 1). The indentation in TBL/MP does not represent a characteristic feature of the winter hemisphere, as discussed above, the events with negative tilts strongly dominate near  $Y \sim 0$  in the YZ- plane in Plate A2. This asymmetry suggests that the interaction of the MSH flow can be different for the negative and positive tilts.

In a case study on June 19, 1998, which stimulated the TBL tilt-dependence explorations, Savin *et al.* (2002a) have demonstrated that Polar registered TBL at about twice smaller Z in the northern/summer hemisphere as compared with the simultaneous southern/winter TBL encounter by Interball-1. Another outlined difference is the existence of the large-scale demagnetized 'plasma ball' inside the southern MP. Before discussing the 'plasma ball' statistics, illustrated in Plates A3 and A4, we are to turn to the case on June 19, 1998, which provides the basis for revision of the cusp throat structure (Figure 1) at the negative tilts (Plate B10).

#### **4 TURBULENT BOUNDARY LAYER AND 'PLASMA BALL' ON JUNE 19, 1998**

We have chosen June 19, 1998 for illustration of the recent findings at the MSH/cusp interface as in those day the ISTP spacecraft provided unique high-resolution synchronized data in the dayside critical regions at the magnetospheric border: Geotail provided high-resolution SW magnetic field and synchronization with WIND plasma data, WIND gave reliable SW plasma parameters, Polar traced northern (summer) stagnation region, Interball-1 entered southern cusp from MSH in high-resolution mode for plasma and field devices. Moderate SW disturbances didn't change dramatically the interaction pattern near MP but were quite helpful in correlation with the Polar and Interball-1

data outside MP and even in determination of the MP per se. The multipoint data interlink has been done with the usage of Gas Dynamic Convention model (GDCF), that is described in details in Dubinin et al. (2002). In spite of several recent papers, describing some features of this event (Savin et al., 2002a, 2002b, 2003b, Khotyaintsev et al., 2003), analysis of modern Cluster data inspired some new findings in the interaction pattern.

#### 4.1 INBOUND MAGNETOPAUSE CROSSING

We start from the upstream Geotail data in Plate A5, where wavelet spectrogram (see details in Savin et al., 2002b) of IMF GSE By-component is shown for 1.6- 100 mHz range (frequency scale in Hz and color scale for logarithm of wave power in  $[\text{nT}^2/\text{Hz}]$  on left side). One of the standing-up problems is to distinguish dynamic interactions of the solar wind with MP from the local disturbances. To shed a light on that problem we compare the Geotail data with that of Interball-1, given on panel i in Plate A6. Both data sets have been processed by the same SWAN tool from LPCE, Orleans with the same parameters (excluding larger frequency range in Plate A6). Black line on panel i in Plate A6 represents  $B_x$ -variation for 2-minute intervals from 4 Hz-sampling magnetic field (scale on right side in  $[\text{nT}/\text{Hz}^{1/2}]$ ). MP crossing (from MSH to cusp, see discussion below) is marked on the Plate A6 bottom along with Interball-1 position in GSM frame in two points. ). On panel a of Plate A6 we display energy densities in  $[\text{eV}/\text{cc}]$ : ion thermal  $n \cdot T_i$  ( $n$  and  $T_i$  - ion density and temperature) – blue line; DC magnetic  $|B|^2/8\pi$  – violet line; kinetic  $W_{\text{kin}}$  - black line, the red curve presents GDCF predictions for  $W_{\text{kin}}$ , multiplied by factor 0.8 to adjust the measured value in the middle MSH (following (Savin et al., 2003b) the time lag is chosen for best fit at 08:40-09:50 UT, while it is certainly different for 07:30-08:30 UT, see Dubinin et al. (2002) and Figure 5 below). Panel b shows electric field ( $E_n$ , black line), calculated from vector product of ion velocity and magnetic field, along the MP normal ( $N \sim (0.7, 0.07, -0.71)$  in GSE frame, see Savin et al 2002a,b) and that of Poynting vector  $P_n$  at 5-50 mHz (blue line). The GDCF proxy for  $E_n$  is labeled by red color, it is shifted by 1 mV/m for the better adjustment with the experimental data. On panel c the magnetic field clock angle in degrees is presented: black line is for the Interball-1 data, violet line – SW monitoring by Geotail, shifted in time to adjust the average Interball-1 data at 09:30-10:00 UT, red line – predictions of GDCF at the Interball location. All three curves correlate at  $\sim 08:40$ -09:50 UT, proving MSH encounter (remember different time lag for earlier period, mentioned above). Panel d displays  $|B|$  in the same format (scale for SW in nT - on right side), systematic discrepancy between the data and SW proxy is blue shadowed, being called ‘plasma ball’ (PB). Note at  $\sim 09:33$  UT similar field depletion, predicted by GDCF: only application of the model provides the reliable tool to determine crossing of the low-shear MP ( $\sim$  at 09:53 UT), imbedded into turbulent boundary layer (TBL, see 3 bottom panels and (Savin et al., 2002a,b)). Change of the ion velocity sign (+/- signs are marked by green/blue color) on panel e ( $V_{ix}$ , GDCF – red line, scale in  $[\text{km}/\text{s}]$ ) conforms the MP encounter. On panel f ion temperature  $T_i$  slightly reduces prior MP and then rises in 1.5-2 times. The reduction reflects only diminishing of the effective temperature of the core MSH ions as the  $T_i$  is fitted to the 3D Maxwellian ion distribution, the  $T_i$  does not account correctly the input from higher-energy protons, clearly seen on panel h since 08:53 UT. The similar remark is also applicable for the absolute value of  $nT_i$  on panel a. On panels g and f electron and ion color-coded (scales for counts per second on the left side) energy spectrograms are presented, the energy per charge scales in eV are depicted on the left. Black lines give count rates of ions and electrons with energies  $> 30$  keV, which flow generally towards the Sun (count rate scales on the right vertical axes). Panel j of Plate A6 depicts wavelet spectrogram of the ion kinetic energy density, panel k – that of thermal ion energy. On Panels l-n we present color-coded (see logarithmic scale on the left side in  $[\text{cm}^{-2} \text{keV}^{-1} \text{ster}^{-1} \text{s}^{-1}]$ ) spectrograms of soft energetic particles for ions flowing from the Sun (FOV 180 degrees from the Sun, cf. black line on panel h), towards the Sun (rotating FOV at 62 degrees from spacecraft spin axis, pointed to the Sun) and anti-sunward flowing electrons (panel n, FOV 180 degrees, cf. black line on panel g).

Returning to comparison of the By-spectra from Geotail and Interball-1 (Plate A5 & Plate A6, panel i), the time lag between Geotail and Interball-1 should be in the limit of 5-20 minutes (Savin et al., 2002a). Within those lags a SW disturbance at ~ 07:52 UT on Interball-1 is quite similar to that of Geotail. In the middle of MSH at ~ 08:30 UT another disturbance practically coincides with that of SW, the low-frequency part is strengthened in MSH. At 09:00-10:50 UT in the MP vicinity wide-band Interball-1 fluctuations are seen, most of them have no counterparts in SW and vice-versa. It implies that the SW driving is not dominant for the near-MP period, analyzed below. Note multiple spectral maximums in this region, called 'TBL' (Savin et al. 1998a, 2001, 2002a,b), which are tied in a complicated manner. As at frequencies higher than 0.7 mHz the disturbances in the TBL have higher level and different frequency dependence, as compared with MSH, we think that the MSH also is not the major source for the fluctuations in TBL. General correlation in magnetic field components and magnitude at 10-11 UT is less 0.5, while sharp IMF changes usually have counterparts in Interball data even inside MP: e.g. Bz disturbance at 10:26-10:32 UT on Interball corresponds to that of IMF Bz on Geotail, shifted by the SW travel time of ~10 minutes, correlation is ~ 0.7.

Just inside the MP energetic electrons have high count rate (Plate A6, panel g), that marks the closed magnetospheric field lines that provide an extra support for placing the PB inside MP (Savin et al., 2003b). Waves in 2-50 mHz range (panels i-k) correlate with intensity of energetic protons (panel h) upstream MP starting from ~08:53 UT. Main wave bursts have counterpart in energetic electrons. The low-shear (~ 80 degrees) PB encounter takes place at tilt ~ - 21 degrees (i.e. the Southern dipole axis being turned from the Sun towards the tail), IMF Bz turned to positive value in about 10 minutes prior to MP. Ion plasma beta at 09:56- 10:03 UT exceeds 15, in the rest blue- shadowed sites it exceeds 2. Similar PB encounters occur on one previous and two following Interball-1 orbits on June 15-27, 1998 (Savin et al., 2003b). Simultaneous Polar data on June 19, 1998 in the northern stagnation region (see Plate B7 and discussion below) demonstrate an open stagnation region with magnetic field controlled by IMF at almost twice smaller |Z| (Plate B9), that implies different OT topologies: its openness for direct interaction with MSH flow at positive tilts in the northern hemisphere and closure by the MP at about nominal position at negative tilts (Savin et al., 2002a). We will return to the PB general properties and statistics in the following section 5.

#### 4.2 DIRECT INTERACTION OF THE MAGNETOSHEATH FLOW WITH 'PLASMA BALL'

After brief discussion of the main previous findings on June 19, 1998, we would like to do detailed insight into TBL properties at negative tilt and at low magnetic shear MP. The main physical problem to address is how practically demagnetized PB (ion beta ~ 15) is interacting with the incident MSH flow in the collisionless plasma? Due to the high beta both in MSH and PB (see blue and violet traces on panel a in Plate A6), the magnetic forces are small and only local electric fields and waves can provide the MSH flow turn and/or dissipation. Note that, as mentioned above, the drop of the thermal energy level at ~ 09:50 UT is at least partially artificial as the  $T_i$  does not include contribution from the higher-energy population, that infers beta>1 at this time as well (in a case of such total pressure drop at MP, the MP should move inside, that contradicts the positive Poynting vector spike on panel b, see details below).

We have chosen the normal to MP electric field (Plate A6, panel b) for presentation as it can be supported by a surface charge at MP-related current sheet(s) and it can deflect the incident MSH plasma to flow along MP, while it can't stop the normal flow in the absence of wave-induced effective collisions. That 'local'  $E_n$  should be seen as regular difference between the measured and SW-induced field (i.e. GDCF one). The MP transition at ~ 09:53 UT is manifested in the permanent change of  $E_n$  sign compared to the GDCF one. Panel b shows that the difference between respective black and red traces is mostly wave-like, while a systematic difference is visible upstream MP at 09:45- 09:53 UT. Such negative  $E_n$  (relative to the GDCF one) might contribute to the flow turning but it should accelerate the incident particles towards MP (instead of repelling) if the measured high-

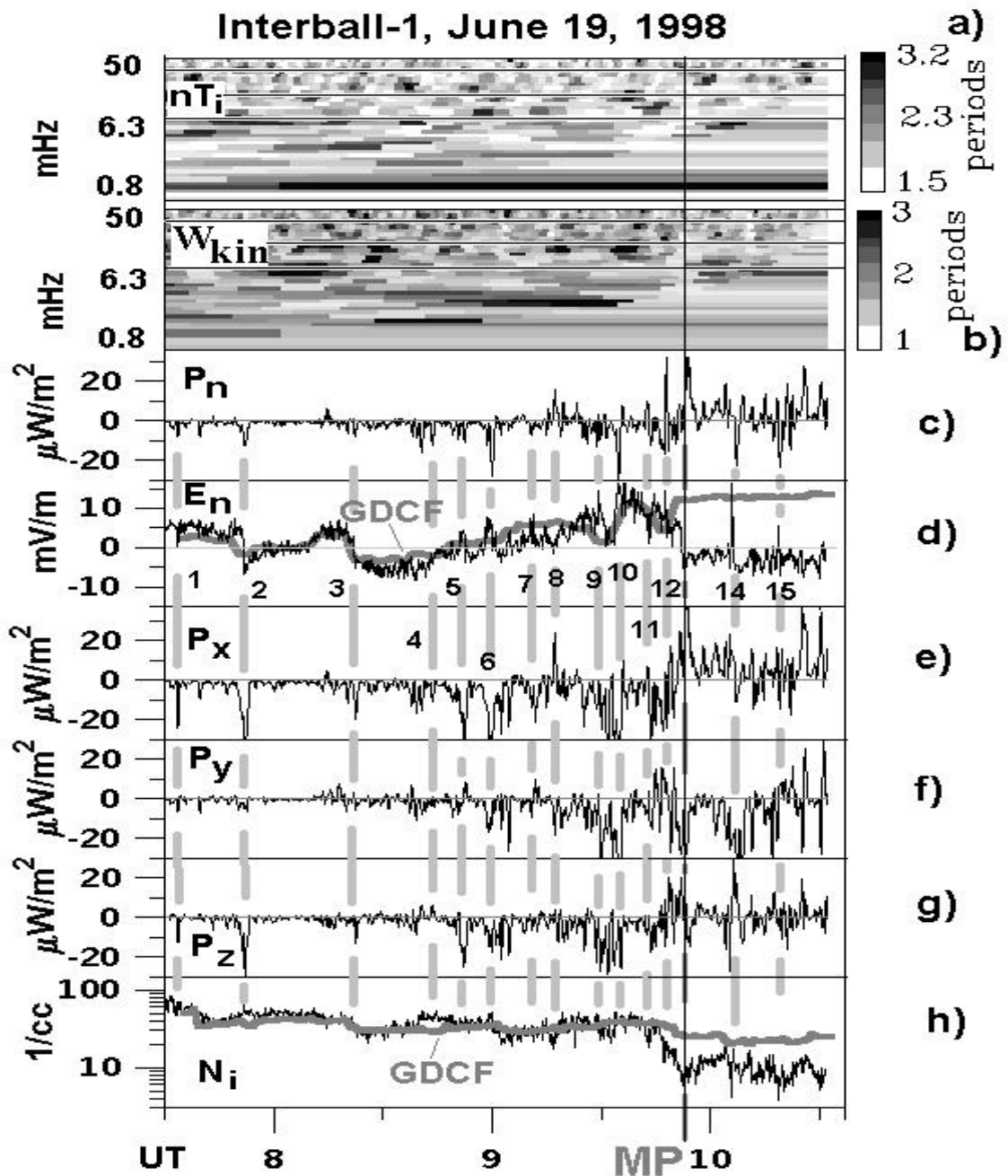


*Fig. 5. Tracing of disturbances in TBL on June 19, 1998; black vertical line – approximate MP crossing. (a) and (b) wavelet correlation time for ion thermal and kinetic energy densities, left – frequency scale in mHz, right – gray scale in periods of coherent signal at every frequency, black horizontal lines – 1<sup>st</sup>, 2<sup>nd</sup> and 4<sup>th</sup> spacecraft spin harmonics; (c) Poynting flux along MP normal (see Plate A6 and related discussions) for 2-50 mHz; (d) electric field along MP normal and its GDCF prediction (thick gray line), the time lag at 08:30-10:30 UT is the same as in Plate A6, the lag at 07:30-08:30 UT is on 7.5 minutes less (numbers mark events discussed in the text); (e-g) Poynting flux along GSE X, Y and Z for 2-50 mHz; (h) ion density and its GDCF prediction (thick gray line), the time lag at 08:30-10:30 UT is the same as in Plate A6, the lag at 07:30-08:30 UT is on 7.5 minutes less.*

amplitude waves provide effective perpendicular conductivity. Thus, we would conclude that the waves should be the major means for the boundary and MSH plasma interaction in the case under study.

In the high-beta MSH-origin plasma we should look at the dynamics of the ion energy rather than at that of magnetic field one (while the latter provides reliable measurements in much larger bandwidth). So, we add spectrograms of the ion kinetic and thermal energy densities to the traditional magnetic field one. We also show behavior of the Poynting flux different components in Figure 5. On its panel a and b we present wavelet correlation times (see Savin 2002b and 2003a for details) for the thermal and kinetic ion energy densities in the same frequency scale as in Plate A6; the difference is that in Plate A6 the analysis intervals (which depend on the frequency) have no overlapping, while in Figure 5 the interval overlapping is 70%. The correlation time indicate how many periods (at each frequency) the signal is coherent; usually signal, conserving coherence for more than 2 periods at several consecutive analysis intervals, can be regarded as regular or quasi-coherent. Panels c, e-g display Poynting vector normal to the MP and its GSE components in frequency band 2-50 mHz versus 5-50 mHz in Plate A6, the latter serves to outline the sunward moving disturbances (i.e. in positive  $P_n$  -direction), which have higher frequency and are partially masked in Figure 5 by the tailward ones with higher power at lower frequencies. On panel d we repeat the normal electric field component for reference to the SW-induced and local disturbances (i.e. different from the GDCF ones), note the different time lags at 07:30-08:30 and 08:30-10:30 UT (see the figure caption). On panel h of Figure 5 the measured and GDCF ion densities are depicted with the same time lags as on panel d. Thick gray vertical lines with interrupts mark characteristic disturbances to be discussed, they are numbered on panels d and e (the MP-related number is omitted).

At 07:30-08:20 UT strong post-shock activity is well seen on panel j (Plate A6, cf. Savin et al., 2002b). Both the spectral and correlation time maximums at 1-2 mHz are recognizable throughout MSH (panel j, k in Plate A6 and a, b in Figure 5). Savin et al. (2002 a, b) outlined similar maximum in magnetic spectra on Interball and Polar at these times, but they couldn't detect continues or coherent signals: its occurred visible in ion energy (pressure) dynamics. The coherence is most prominent on panel a of Figure 5.

At 08:35-08:53 UT some weak activity on panels i-k (Plate A6) is also seen, but it resembles that of Plate A5 and thus could be SW- driven. The respective maximum at  $\sim 4$ -5 mHz in correlation time (panel b, Figure 5) could be traced from the post-shock region at 07:50 to 08:50 UT (with frequency changes at events 2 & 3, driven by SW, see panel d, Figure 5), where it is masked by the strong local maximum at  $\sim 3$  mHz (see discussion below).

We pay main attention to the disturbed region upstream MP at 08:50-09:50 UT. This region is characterized by strong disturbances, which are not the SW-driven ones (Plate A5, panels a-e & i-k in Plate A6). Soft energetic ions are registered there (panels h, l, m, Plate A6), which can't be accounted exclusively by the leakage from the southern magnetosphere along locally reconnected field lines (see respective discussion in section 4.6 and Savin et al., 2003b). Appearance of those particles correlates with the strong energy fluctuations and with drop of the MSH kinetic energy. The latter drop is well seen from 09:57 UT on panel a in Plate A6 as systematic difference between black and thick red traces (remember, that another difference at  $\sim 08:25$  UT is due to different time lag at this time, which is taken into account in Figure 5). Panel e also demonstrates the growing departure of  $V_{ix}$  from the model since that time. While ion velocity (especially  $V_{ix}$  – the main velocity component in MSH) is measured on Inrerball-1 accurately enough, the density should be cross-checked. We do that on panel h in Figure 5: the average density follows the GDCF proxy rather well till the diffuse MP encounter with two exceptions at  $\sim 07:50$  and  $08:45$  UT. We have skipped the former post-shock one (which can be affected by a partial shock crossing), and checked for the latter the ion momentum  $n_i * V_{ix}$  : at those time it is close to the GDCF prediction, while departs since  $\sim 09$  UT. It confirms the reliable  $n_i$  measurements and so, the local dramatic  $W_{kin}$  dissipation (as the GDCF proxy is slightly rising instead of falling) after 09 UT.

In MSH upstream the TBL at 08:40-08:50 UT the standard deviations of the ion energies are:  $\delta W_{kin} \sim 22\%$ ,  $\delta nT_i \sim 10\%$ . As we've mentioned above, the ion thermal energy absolute value should be corrected by taking into account the soft energetic particles input, thus the total energy density (pressure) balance at  $\sim 09$  UT should be improved. Any case, panel k in Plate A6 displays that namely at the TBL external boundary at  $\sim 08:53$  UT the ion thermal energy density (i.e. proportional to the ion pressure) starts to fluctuate till 09:35 UT, at 09:03-09:15 UT the thermal disturbances dominate over that of  $W_{kin}$  (outer TBL zone, OZ),  $\delta W_{kin} \sim 49\%$ ,  $\delta nT_i \sim 20\%$ ,  $\delta W_{kin}/\delta nT_i \sim 0.48$ . At 09:35-09:50 UT the ion kinetic energy fluctuations relatively dominate (the inner zone, IZ, see panel j),  $\delta W_{kin} \sim 60\%$ ,  $\delta nT_i \sim 35\%$  (mostly due to the linear trend, i.e. change of the average value),  $\delta W_{kin}/\delta nT_i \sim 0.76$ . In the middle of upstream TBL both kinetic and thermal ion energies are quite disturbed (09:15-09:35 UT, the middle zone, MZ),  $\delta W_{kin} \sim 71\%$ ,  $\delta nT_i \sim 25\%$ ,  $\delta W_{kin}/\delta nT_i \sim 0.996$ . Relative to the upstream MSH average values (08:40-08:50 UT) the standard deviations in the MZ are:  $\delta W_{kin} \sim 45\%$ ,  $\delta nT_i \sim 17\%$  (close values are for 08:53-09:50 UT interval). The low limit for the energy conversion into the irregular fluctuations in the TBL prior to MP is 23% of MSH kinetic energy and 7% of its thermal one (i.e. the difference of standard deviations). As the TBL spectra on panels j and k are quite different from the upstream MSH ones, we tend to accept the upper limits for the MSH energy chaotization - of  $\delta W_{kin} \sim 40\%$  and  $\delta nT_i \sim 15\%$  (without accounting the upstream MSH fluctuations with different from TBL spectra). There is still one puzzling problem in OZ: strong deficit of the average  $W_{kin}$  (and respectively, of the momentum as  $n_i \sim \text{const}$ , see Figure 5, panel h), even sum of  $W_{kin} + \delta W_{kin}$  at 09:03-09:15 UT constitutes only 47% of the average upstream  $W_{kin}$ . The only candidate to carry out the momentum

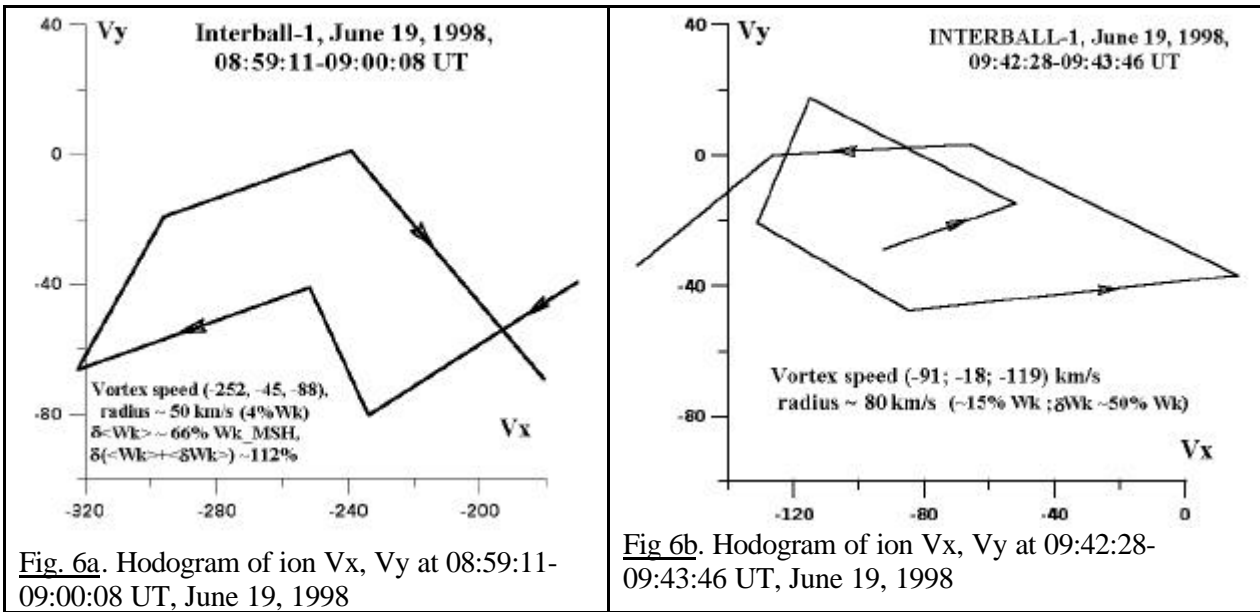


Fig. 6a. Hodogram of ion  $V_x, V_y$  at 08:59:11-09:00:08 UT, June 19, 1998

Fig 6b. Hodogram of ion  $V_x, V_y$  at 09:42:28-09:43:46 UT, June 19, 1998

and kinetic energy excess is the strong impulse in the  $W_{kin}$  and  $V_{ix}$  on panels a, e and j at  $\sim 09$  UT. Respective hodogram of the ion speed vector tip in the plane of GSE ( $V_x, V_y$ ) is shown in Figure 6a. The average speed in the depicted interval 08:59:11- 09:00:08 UT is (-252, -45, -88) km/s, possible inferred vortex component (i.e. the loop in the hodogram) has radius of  $\sim 50$  km/s ( $\sim 4\%$  its average  $W_{kin}$ ,  $W_{kin}$ -pulse exceeds even local  $nT_i$  on panel a in Plate A6), the standard deviation  $\delta W_{kin} \sim 66\%$  average  $W_{kin}$  in the upstream MSH, the sum of deviation and average  $W_{kin} + \delta W_{kin} \sim 112\%$  average MSH  $W_{kin}$ . A magnetic loop at this time has been found only at  $\sim$  twice lower frequency. This plasma jet in Plate A6 is in the middle of a current sheet (bi-polar disturbance in the clock angle), it is bounded by  $|B|$  drops down to few nT ('diamagnetic bubbles') and bi-polar  $E_n$

spike ( $\sim 5$  mV/m), which can be accounted by surface charges at the current sheet. In Figure 5 it is event 6, which contains the impulsive density rise. The negative spike of Poynting flux in all components (for 5-50 mHz GSE vector being  $(-20, -6, -5)$   $\mu\text{W}/\text{m}^2$ , i.e. at  $\sim 24$  degrees to the model speed  $(-247, -6, -157)$  km/s, departing from the model flow towards  $-X$  and  $-Y$  directions) in the event 6 conforms the energy pushing downstream by this strong nonlinear structure, the  $P_n \sim -10$   $\mu\text{W}/\text{m}^2$  (positive means outward MP along its normal, see panel c, Figure 5 and panel b, Plate A6 for 2-50 and 5-50 mHz ranges respectively) indicates approaching of the disturbance to the MP. The latter excludes a near-MP reconnection as a mechanism for the jet acceleration: (a) any MP-related disturbance should move outward MP (i.e. it should have the positive  $P_n$ -spike); (b) the distance from the MP is too big (in  $\sim 1$  hour prior its crossing), the GDCF does not predict substantial outward MP moving in this period; (c) negligible  $|B|$  just inside MP and in its vicinity (magnetic energy density is in about an order of magnitude less that of the  $W_{\text{kin}}$  spike in event 6) can hardly result in so strong plasma flow acceleration up to Alfvénic Mach number  $\sim 3.1$ .

As the Poynting flux is crucial for the TBL mechanism determinations, we would like to discuss the reliability of its measurements and correctness of the electric and magnetic field filtering prior to the Poynting flux calculating. First of all we call your attention to events 2 and 3 in Figure 5 on panel d: the measured  $E_n$  fairly well reproduces that of GDCF (cf. magnetic field etc. in Dubinin et al., 2002). Thus, these events represent SW disturbances moving downstream MSH far from the disturbed TBL. Accordingly, all Poynting flux components are negative in these events, that conforms the downstream MSH flow (cf. Interball-1 GSM position, given in Plate A6 at 09 UT,  $(3.7, -2.1, -10.7)$   $R_E$ ). The same is most probably valid for events 1, 4 and for the low-frequency  $E_n$ -trends between events 9-10 and 11-12 (that corresponds to the GDCF  $E_n$ -trends, we have checked the same with the magnetic field as well). So, the moderate SW disturbances provide a validation for our Poynting flux measurements in MSH.

Turning back to the TBL in Figure 5, between event 4 and MP one can see strong enhancement in appearance of the negative (downstream)  $P_x$ ,  $P_y$  and  $P_z$ -spikes, events 5-7 and 9 correspond to local TBL disturbances in Plate A6 without correlative features in SW (Plate A5). Similar to the event 6, the events 5, 7, 9 have related clock angle and electric field spikes, while the event 6 is unique for the plasma jetting. There is another group of perturbations with positive  $P_n$ -spikes, i.e. moving from MP towards the outer TBL border: number 8, 10-12 and MP. They and have shorter time duration and thus are better visible in Plate A6, where the lower frequencies  $<5$  mHz have been filtered out. The  $P_n$ -positive events dominate in IZ, the 12<sup>th</sup> one has even positive  $P_y$  and  $P_z$ , moving upstream along MP. The MP-related perturbation moves in positive  $X$  and  $Z$  but in strongly negative  $Y$  directions. Event 14 inside MP resembles short double MP crossing, but generally moves from MP (negative  $P_n$ ) as the event 15 does, the  $P_y$  and  $P_z$ , for the former are similar to that of MP. The MZ contains a mixture of the local inward and outward moving events. In the OZ between events 6 and 7 weak positive  $P_n$ -spikes of short duration could be distilled yet.

The ion velocity hodogram in GSE plane ( $V_x, V_y$ ) for the trailing part of event 11 with negative components of Poynting vector is depicted in Figure 6b. The average speed in the interval 09:42:28- 09:43:46 UT is  $(-91, -18, -119)$  km/s, the inferred vortex component has radius of  $\sim 80$  km/s (i.e. 15% its average  $W_{\text{kin}}$ ), the standard deviation without the linear trend  $\delta W_{\text{kin}} \sim 44\%$ . Thus, the vortex energy is big enough for a nonlinear wave, it contains  $> 1/3$  of the chaotic kinetic energy. No obvious vortex-like magnetic loop has been detected around event 11.

Correlation times in Figure 5 provide information on the disturbances coherence.  $W_{\text{kin}}$  ‘synchronization’ at  $\sim 5$  mHz (09:15 –09:45 UT) corresponds the appearance of the positive  $P_n$ -spikes in MZ. I.e. the reflected (sunward going) wave packets seem to ‘organize’ interactions in the closest to MP upstream region. In the OZ and just upstream (08:45-09:35 UT, events 4-10), where strong maximum at  $\sim 3$  mHz in  $W_{\text{kin}}$  correlation time, most probably, results from regular launching of the tailward packets from the outer TBL boundary. They could be in turn triggered by interaction of the up-going waves with the regular MSH flow at this boundary and/or in its vicinity. The

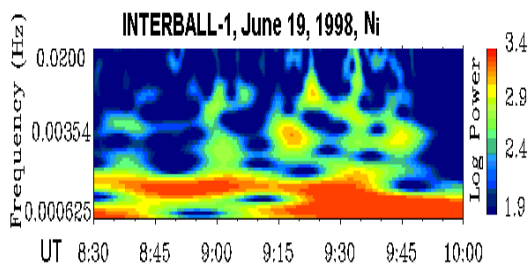


Plate B1. Spectrogram of ion density, June 19, 1998

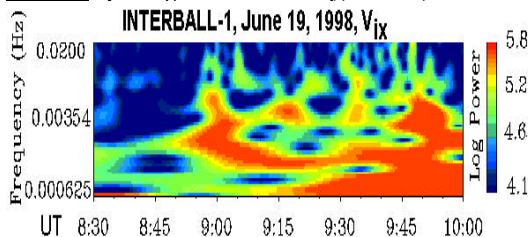


Plate B2. Spectrogram of velocity  $V_{ix}$ , June 19, 1998

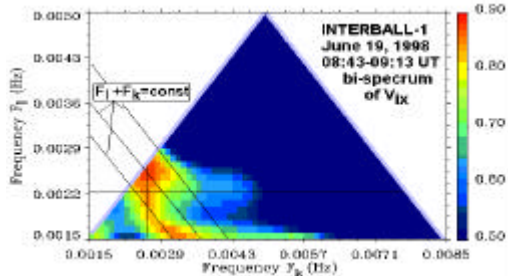


Plate B3. Bi-spectrum of velocity  $V_{ix}$ , 08:43-09:13 UT

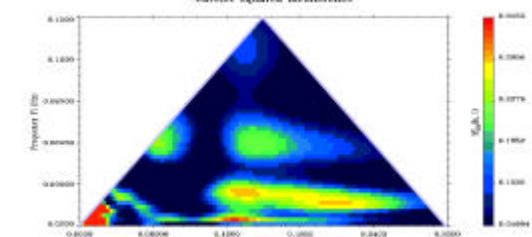


Plate B4. Bi-spectrum of  $B_x$ , 09:16- 09:50 UT

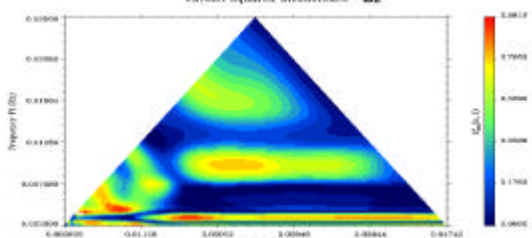


Plate B5. Bi-spectrum of  $B_z$  from the kinetic model

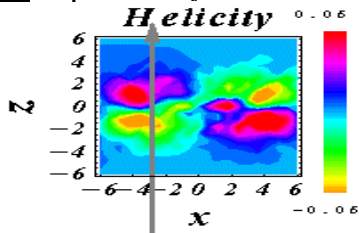


Plate B6. Helicity for the kinetic model current sheet

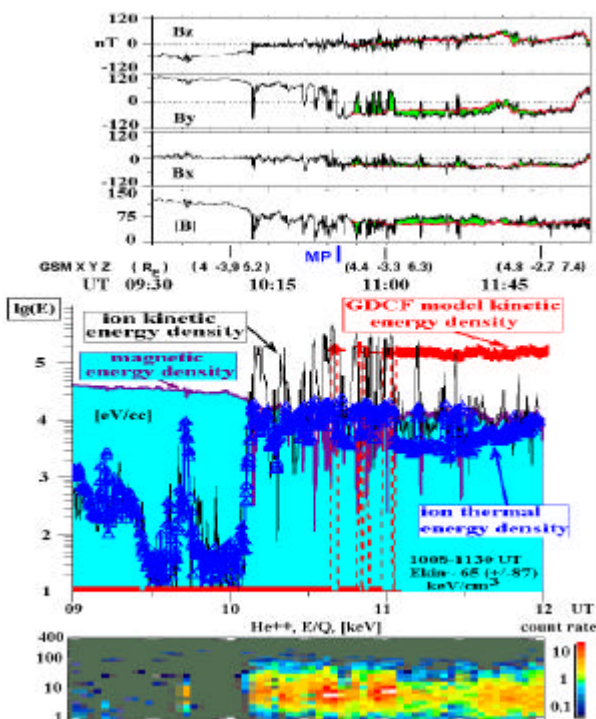


Plate B7. TBL crossing by POLAR, June 19, 1998. Top: GSM magnetic field versus GDCF (red line). Middle: Magnetic (blue-shadowed), thermal (triangles) and ion kinetic (GDCF - red line) energy densities. Bottom: He++ spectrogram

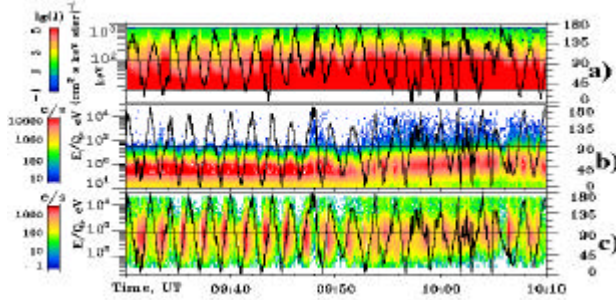


Plate B8. Ion and electron (b) spectrograms and pitch-angles (right scale), Interball-1, 09:30-10:10 UT, June 19, 1998.

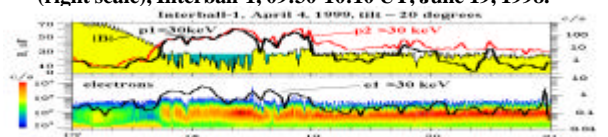


Plate B9. Open OT, April 15, 1999. |B| (top, yellow-marked) & protons (>30 keV, p2 (red)- from Sun, p1- towards Sun); electron spectrogram & intensity (>30 keV, towards Sun)

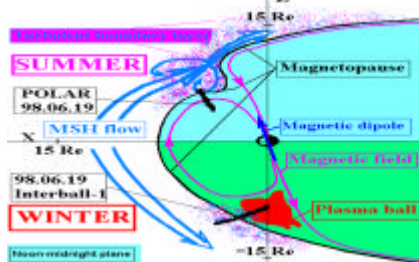


Plate B10. Sketch for MSH interaction with cusps

maximum at 3 mHz is also seen on panel a in Figure 5. Under MP the quasi-coherent signals are at  $\sim 7$  mHz, that corresponds to Pc4 pulsations. Coherent bursts at 14-17 mHz are visible at the MZ borders (events 8 and 10); the  $nT_i$ - one corresponds event 6. Events 4 and 11 contain a coherent substructure in  $nT_i$  at  $\sim 10$  mHz. The PB just inside MP is characterized by the quasi-coherent packets at 6-7 and 10 mHz.

To give more details for the upstream TBL interactions we blow-up interval 08:30-10:00 UT in Plates B1 and B2, showing wavelet spectrograms for the ion density and velocity  $V_{ix}$ , respectively. The former is similar in main features to panel k in Plate A6, but it doesn't contain uncertainties in  $T_i$  calculations, mentioned above. The latter is quite compatible with panel j in Plate A6 and provides the direct comparison with a bi-spectrum in Plate B3 (bi-spectra of  $W_{kin}$  are smeared by the double-frequency maximums from  $V^2$ -factor). Plate B1 demonstrates strengthen of the low-frequency ( $\sim 1.3$  mHz) maximum just upstream the plasma jet at event 6 (09 UT), the coherent signal at 4-5 mHz (panels a, b, Figure 5) can be relayed with a weak maximum at  $\sim 4.2$  mHz. Referring on Poynting flux in Plate A6 and Figure 5, we would conclude that the weak waves at  $\sim 4.2$  mHz, going upstream, (see small amplitude and duration bursts in  $P_n$  on panel b in Plate A6) trigger amplification of the down-going low-frequency waves. The former weak maximum is visible at 08:4-08:55 UT in Panel B2 along with the stronger one with rising tone from  $\sim 1.5$  to 2 mHz. The latter grows further in magnitude and frequency ( $\sim 2.3$  mHz) until 09 UT (i.e. until event 6 and plasma jet launching), where it bifurcates onto rising- and falling- frequency tones, which evolve toward about 1.3 and 2.7-3.5 mHz bands (cf. correlation time maximums on panels a, b in Figure 5). At  $\sim 09$  UT maximums at about 5.5 and 11-12 mHz are also visible. Thus in the upstream TBL at 09:00-09:45 UT the mentioned above kinetic energy drop results not only in the plasma jetting but also in amplification of the low-frequency pulsations ( $\sim 1.3$  mHz), three periods of which ( $\sim 15$  minutes) cover almost whole upstream TBL, these fluctuations correspond to maximums at 3-10 mHz at  $\sim 09:00$ , 09:15, 09:30 and 09:45 UT. It conform a the 'thick' TBL transition invoked by Savin et al. (2001) versus a 'thin' shock-like one, i.e. a macro-equilibrium could be not achieved in the outer BL during few its characteristic periods (and, probably, throughout few characteristic wave-lengths).

To check if the outer TBL processes are really synchronized we analyze the wavelet bi-spectrum (bicoherence) for the velocity  $V_{ix}$  in Plate B3, which correspond to a frequency sum rule for the 3-wave process,  $f_s = f_l + f_k$ . The bicoherence has substantial value only if three processes, with the highest frequency being the sum of the rest two, are phase-coupled (cf. Savin et al. (2002b)): the module of the product of 3 complex wavelet amplitudes is normalized by the modules of amplitude of the three signals at respective frequencies. We assume that the most-powerful non-linear 3-wave process (excluding the harmonics) in the TBL is decays (or junction), which requires the third-order non-linearity in the system. The weaker, higher-order non-linear effects, which also might contribute in the TBL physics, are beyond the scope of this paper and will be addressed in future studies. In Plate B3 we display the bicoherence of  $V_{ix}$  at 08:42:57-09:12:51 UT for  $f_k \sim 1.5$ - 8.5 mHz (the larger frequency in the sum) and  $f_l \sim 1.5$ -5 mHz (the lower limit is determined by the time interval of analysis). The horizontal and vertical black lines indicate processes with nearly constant  $f_l$  and  $f_k$ , respectively, the negatively inclined lined mark processes with  $f_s = f_l + f_k \sim \text{constant}$ . Note, that we show only processes with the relative amplitude  $> 0.5$  (50% of the triple product absolute value), i.e. all colors, except the dark blue background, mark the signals with the bicoherence certainly above a noise (cf. maximum bi-spectral amplitudes  $\sim 50\%$  in Savin et al. (2001, 2002a, b, 2003a)).

Neglecting the frequency drifts near the bifurcation point at 09 UT in Plate B2, we can distill the processes in Plate B3 at several frequencies:

- $f_l \sim 1.5$  mHz, lower horizontal maximum, cf.  $\sim 1.3$  mHz in Plate B2 and in Figure 5;
- $f_l \sim 2.3$  mHz, upper weak horizontal maximum, compatible with the general upstream maximum at 08:50-09:00 UT in Plate B2;

- $f_s = f_1 + f_k \sim 4.5$  mHz (the lower inclined line), which is close to the upper downstream maximums at 09:10-09:40 UT in Plate B2 and to that of upstream maximums in Plates B1, B2 and Figure 5;
- $f_k \sim 2.6$  mHz, strong vertical maximum (cf. panel b in Figure 5 and Plates B1, B2) with the largest amplitude at its top, the latter red spot corresponds to the second harmonic generation (cf. Savin et al., 2002b), visible at 09 UT at  $\sim 5.5$  mHz in Plate B2. Note, that the upper red spot is wide and invokes also crossing of the 3 mentioned above processes, except the lowest frequency one. The middle inclined line, probably, marks  $f_s = f_1 + f_k \sim 5.5$  mHz.

Another red-spot maximum at the lowest  $f_1$  would infer the wave pumping at  $(f_1, f_k) \sim (1.5, 3)$  mHz with further nonlinear cascading at  $f_s = f_1 + f_k \sim 4.5$  mHz (lower inclined line) and  $f_1 \sim 1.5$  mHz, see the lowest horizontal maximum till 6 mHz (Savin et al., 2001, 2002b). We assume the cascade signatures, e.g. in the case of the horizontal-spread maximum, when at the sum frequency,  $f = f_1 + f_2$ , the bicoherence has comparable value with that at the starting point  $(f_1, f_2)$ , it implies that the wave at sum frequency interacts in turn with the same initial wave at frequency  $f_1$  in the following 3-wave process:  $f_3 = f_1 + f$  etc. Note also horizontal and vertical cascading at the mentioned above frequencies of 2.3 and 2.6 mHz. The linkage between the spectrogram maximums represents a feature of cascade-like processes in Plates A6, B1 and B2.

Thus the bi-spectrum provides strong support for the phase coupling of the low-frequency fluctuations in the upstream TBL. We have also checked the wavelet spectra and bi-spectra for ion density, kinetic and thermal energies and got highlighting of the similar processes up to about 20 Hz. The 3-wave nonlinear wave-coupling persists also in MZ and IZ. Similar to the magnetic spectra in Plate A6, the simultaneous magnetic bi-spectra differ from that of Plate B3: the  $B_z$  one is completely different; in  $B_y$  only 2.3 mHz maximum is present, in wider intervals 1.3 and weak 3.5 maximums are recognizable; in  $B_x$  2.3 mHz maximum is seen along with the 1.3 one at wider interval without the horizontal spread. All magnetic spectra have lower maximum magnitudes (up to 0.5-0.6 instead of 0.9 in Plate B3). In spite of the differences the magnetic spectra are measured in much wider frequency ranges and we use them for the higher frequency studies and for comparison with a kinetic model (see Plates B4 and B5 and discussion below).

#### 4.3 COMPARISON WITH POLAR DATA ON JUNE 19, 1998.

We have discussed the Interball-1 data mostly at negative tilts. Let us briefly compare the case on June 19, 1998 with the simultaneous Polar data in the northern hemisphere (tilt  $\sim 20$  degrees). Referring for details to Dubinin et al. (2002), Savin et al. (2002a, b), we present the Polar outbound crossing in Plate B7. The magnetic field at the Plate B7 top highlights the MSH encounter in  $B_y$  transition from the positive magnetospheric values to the negative MSH ones, which conforms the GDCF predictions (red line, the difference with the measured field is highlighted by green color). We mark MP, which separates average MSH and magnetospheric fields, traverses of MP current sheet may be multiple. Subsequent apparent traversals of current sheets at  $\sim 10:50-11:05$  UT resemble the MP ones, but their spectra are different, being similar to that of Interball in TBL (see Figure 7 and discussions below). We attribute these intense fluctuations to TBL. Note the MP being at GSM  $Z \sim 6 R_E$  versus  $-10 R_E$  for Interball-1 (see Plate A5), the respective orbit traces are given by thick black lines in Plate B8. In the middle panel of Plate B7 we display the energy densities similar to Plate A6. The spiky bursts of the kinetic energy density (black line) have been attributed by (Dubinin et al., 2002) & (Khotyaintsev et al., 2003) to the reconnection bulges. One can see from comparison with model kinetic energy and between the measured and model magnetic field that the bulges appearance is controlled mostly by the local TBL processes (i.e. no SW driving is proved by GDCF); the micro-reconnection bulges should be modulated by the upstream TBL fluctuations (see discussion in the previous section), as the spectral features of the magnetic fluctuations (in the band of the repetition of the reconnection bursts) in the transition region at 10-11 UT are quite similar to that of measured by Interball-1 in the upstream TBL (see Figure 7 and (Savin et al., 2002a)).

Another feature, which we would like to outline, is  $\sim$ fitting of kinetic energy in the ‘reconnection bulges’ at 10-11:20 UT to the GDCF model predictions (red crosses visible as a thick line on the middle panel), while the magnetic field energy density has much smaller magnitude even inside MP. It implies a substantial difference with reconnection inferred at low latitudes, where the MSH dynamic pressure results first in compression of the static magnetic field and then the magnetic energy is released through the (quasi-static) reconnection into plasma acceleration and heating. At high latitudes with MSH flow, sliding along MP, the TBL-triggered bursty reconnection plays a role of ‘shutter’ (Galperin, 2001), which provides the local transformation of the MSH kinetic energy directly into that of deflected/accelerated flows. Thus, the anti-parallel reconnection in the TBL could play the secondary (but quite valuable) role in the energy and magnetic flux transformation process, as it had been proposed by (Haerendel, 1978).

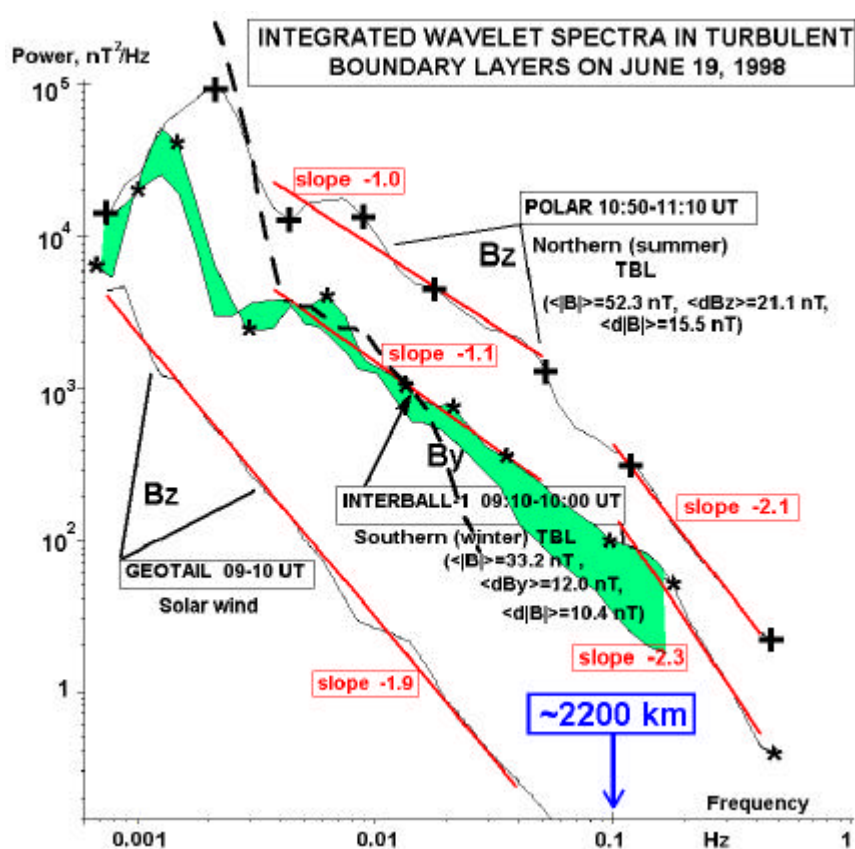
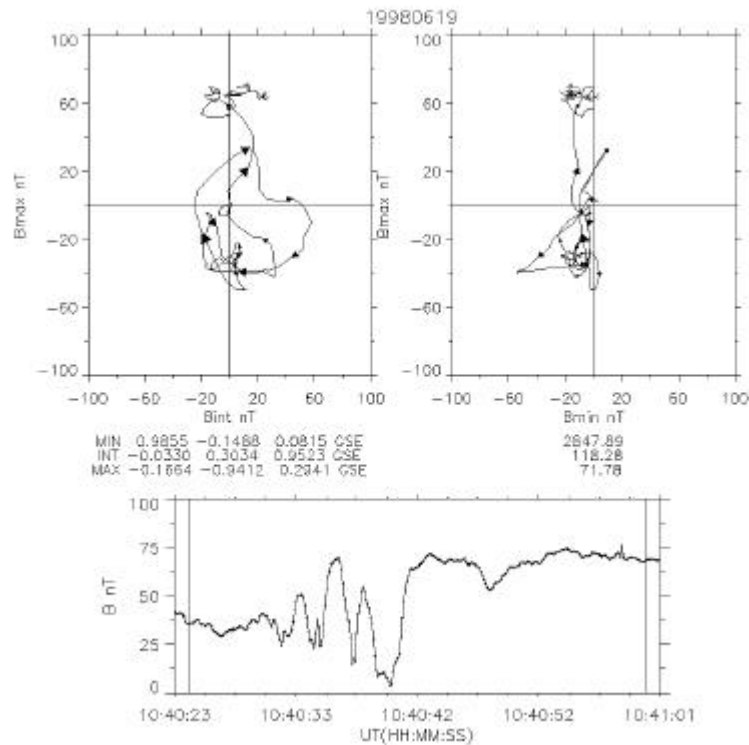


Fig.7. Wavelet integrated spectra in the northern/ southern TBL and in the SW

The example of the accelerated jet in the upstream TBL, which occurred to be incompatible with a reconnection mechanism but synchronizes the quasi-coherent interaction pattern in TBL and results from chaotization of  $\sim 40\%$   $W_{kin}$  in MSH (see event 6 in Figure 5 and Plates A6, B1, B2 and B3 and related discussions above), invokes an alternative explanation for the regular plasma jets, registered by Polar: they originate at the outer TBL border (that’s why they have similar statistical properties to that of TBL registered by Interball-1) and then they interact with the deformed MP over cusp (remember strongly negative  $P_n$  in the event 6). Their extremely high kinetic energy density can provide locally the substantial MP deformation and as a result the secondary reconnection of the perturbed fields. The jet alignment to +Y direction at  $Y \sim -3.3 R_E$  (Khotyaintsev et al., 2003) conforms deflection of an incident flow deep in the funnel-shaped outer cusp throat. For the quantitative comparison of the TBL properties with the SW ones we present characteristic spectra in Figure 7 from the core TBL intervals at 09:10- 10:00 and 09:53- 11:00 UT (shadowed in

between), and compare them with the Geotail SW data at 09-10 UT and with that for the northern TBL entered by Polar at 10:50 – 11:10 UT (Savin *et al.*, 2002b). Two characteristic negative slopes are actually seen:  $\sim 2.3$  at 0.1-0.5 Hz and  $\sim 1.1$  at 0.004-0.05 Hz (note similar slopes at the upper trace with the crosses from Polar). The different slope of  $-1.9$ , seen by Geotail in SW, and the absence of any maximum in the Geotail data demonstrate that the dominant processes in the TBL in this event are the local and inherent ones, in spite of the average field is following the SW. Interball-1 magnetic spectra for 0.004-0.5 Hz shadowed curve without asterisks) have similar shape to that of the core TBL (trace with asterisks), while the slope at 0.004-0.05 Hz of 1.3 is slightly higher. At 09:55- 10:30 UT the slope from Interball-1 at 0.1- 0.5 Hz is the same as in the TBL just outside MP. The characteristic power at low frequencies in the core region is about twice that just inside MP (at



*Fig. 8. Polar encounter of a current sheet in TBL on June 19, 1998. From bottom: Magnetic field magnitude; Magnetic vector hodograms in maximum/ intermediate (left) and maximum/ minimum (right) variance frames*

09:10-10:00 UT, the difference is shadowed). Shifting the interval to 09:56-10:08 UT reduces the peak at  $\sim 0.0014$  Hz by factors of 2 to 3 but doesn't change much the rest of the spectrum. This is in strong contrast to that seen in the summer TBL where the power drops by the order of magnitude in the outer cusp (see (Savin *et al.*, 1998, 2002a,b)). The difference of the power for Polar and Interball spectra in Figure 7 of about one order of magnitude can't be attributed to the higher average magnetic field on Polar ( $\sim$  in 1.6 times). We suggest that the power excess may be due to patchy reconnection of the nearly anti-parallel fields on Polar (cf. (Dubinin *et al.*, 2002)). In the Interball case the average field is not annihilated and the energy input into turbulence is thus lower. Another characteristic TBL feature is the fact that the standard variances  $\langle dB_z \rangle$  and  $\langle dB_y \rangle$  are higher than that of the field magnitude  $\langle d|B| \rangle$  (see text in Figure 7). It implies that the transverse magnetic fluctuations dominate over the compressible ones (cf. (Savin *et al.*, 1998, 2001, 2002a,b)). To estimate the scale of the kink in Figure 7 we have found dHT frame with GSE velocity  $\mathbf{V}_{HT} = (-156, 82, -121)$  km/s and regression  $R = 0.993$  at 09:35:31- 09:39:03 UT. That gives for the kink  $L \sim 2200$  km, that is marked in Figure 7.

In about one third cases in TBL the field rotations contain solitons-like structures which include DBs. In Figure 8 we depict a characteristic example from the Polar data at 10:41 UT in the northern TBL (see details in [Savin *et al.*, 2002b]). The displayed transition contains a quasi-regular structure in  $|B|$  (bottom panel) enveloped by the field, hodogram of which (top panel) resembles a 3D spiral with increasing radius (decreasing with the distance from the main rotation). Note, that the duration of DB wave-train again corresponds to the maximums at  $f_K \sim 0.13$  Hz and to the spectrum kink in Figure 7; the wave-train filling frequency of  $\sim 0.35$  Hz belongs to the high-slope part of the upper spectrum (ion cyclotron frequency being  $\sim 0.45$  Hz for average total field  $\sim 30$  nT trough the structure, see Figure 8). One needs high- time resolution plasma moments to compare properly such transitions with intermediate/ slow shocks from kinetic simulations by e.g. [Karimabadi *et al.*, 1995], while we should mention that the  $|B|$  drop by the order of magnitude does not appear in simulations.

#### 4.4 STATISTICAL PROPERTIES OF MAGNETIC FLUCTUATIONS.

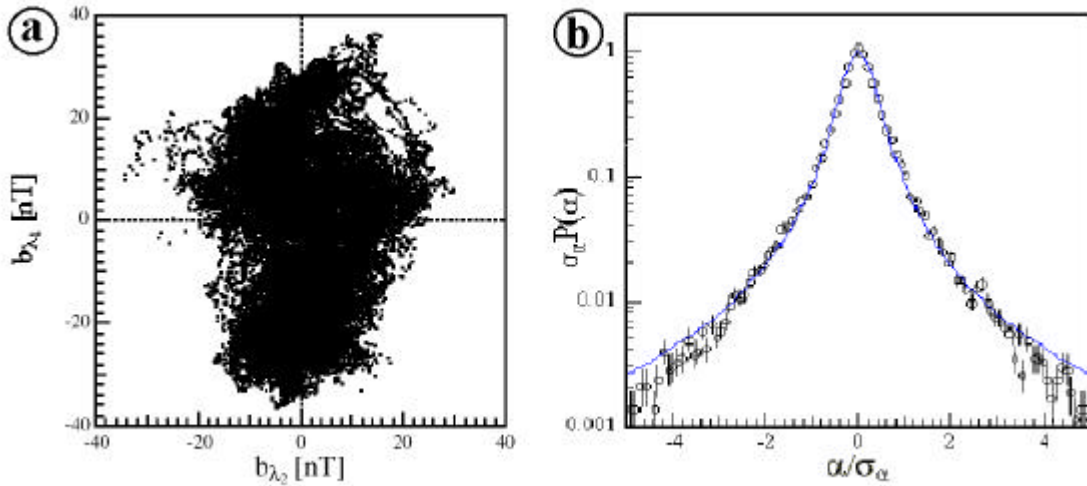


*Fig. 9. Statistical properties of the TBL magnetic fluctuations.*

*a:* The tip of the magnetic vector motion in the maximum variance plane for the TBL period (see bottom panel of Plate 1B),  $\mathbf{I}_1$  and  $\mathbf{I}_2$  refer to the maximum and medium variance directions.

*b:* the normalized probability distribution function of the rotation angle of the magnetic field vector in the maximum variance plane. The solid line refers to a nonlinear best fit using a symmetric Levy-stable distribution function characterized by a characteristic index  $\alpha \sim 1.17$  (see also text).

In Figure 9 we present results of a statistical study of the TBL fluctuation behavior. The tip of the magnetic vector motion in Figure 9a is shown in the maximum variance plane for the TBL period. The field direction variance looks rather random. Visible dividing on the upper and lower parts is both due to changes in average direction of the SW-induced field outside MP and due to the different magnetospheric-controlled field direction inside MP. Note also the difference in the TBL spectral shapes inside and outside MP (shadowed traces in Figure 7). Figure 9b shows the normalized distribution function of the rotation angle of the vector in the maximum variance plane. There is the evidence of a non-Gaussian statistics at the high rotation angles, which is seen as a nonlinear best fit using a symmetric Levy-stable distribution function characterized by a characteristic index  $\alpha \sim 1.17$  (the solid line). The Gaussian distribution should look like a parabola (a Levy-stable distribution function with a characteristic index  $\alpha = 2$ ) in Figure 9. Most probably, the departure from Gaussian distribution should be attributed to the existence of the structures with small-scale current sheets, such as we present in Figure 8. Thus, these solitons-like structures, while appearing as casual crossings of

MP, as surface waves or as reconnection pulses [Dubinin *et al.*, 2001, Savin *et al.*, 2002b], control the spectral shape of the TBL turbulence and change its statistical properties.

#### 4.5 COMPARISON WITH KINETIC CURRENT SHEETS

[Dubinin *et al.*, 2002] and [Savin *et al.*, 2002b] assume that the quasi-regular jets at 10-11 UT represent cusp counterparts of patchy merging. These spiky cusp jets constitute a part of the flow coherent interactions, discussed above. The difference between  $V_{HT}$  and average ion bulk velocity in the jet vicinity is in the limit of the bulk velocity variations (deviation  $< 16$  degrees) that should be a characteristic feature for standing structures in the cusp plasma frame. So, we could infer the space rather than time resonance pattern at the MSH/ cusp interface.  $V_{HT}$  is at 107 degrees to the surrounding magnetic field, then one can get an estimate of transverse scale of the jet of  $\sim 2 Re$ .

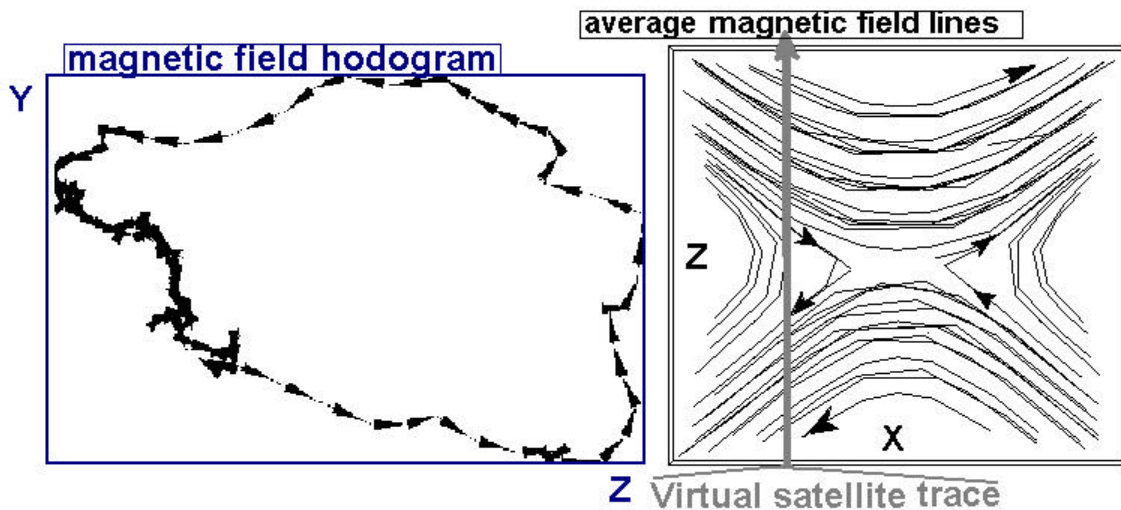


*Fig.10. Virtual satellite trace through the model reconnected current sheet (right panel, see also Plate 1D, 1E, and text) and hodogram of magnetic field, visible on the virtual satellite in the model (YZ) plane.*

To check if the visible features at higher frequencies ( $> 10$  mHz) TBL can be accounted by crossings of thin current sheets at nonlinear state, we compare the experimental data with that of virtual satellite in a model current sheet. We use results of kinetic simulations by [Buechner *et al.*, 1998] of the reconnection, developed in the current sheet between anti-parallel magnetic fields. We depict representative field picture on the right panel in Figure 10. In the initial state the current sheet with gradients in Z direction and external field in X direction has neither Y-dependence nor  $B_y$  – component, no average change of plasma density across the current sheet has been inferred. In Figure 10 we present 2D -case with no Y-dependence and periodic picture in X- direction (i.e. one period in X is displayed). After  $\sim 15$  ion gyro-periods in the external field the current sheet divides into reconnected X- and O- lines: in the Figure 10 one X-line and two halves of O- lines are shown. Unlike MHD, in kinetic simulations strong  $B_y$  –component is generated, that leads to appearance of helicity maximums along the X-axis, as it is shown in Plate B6 for the same region as in Figure 10 (right panel, see details in (Savin *et al.*, 2002b)), the X and Z axes are normalized here by half-width of unperturbed current sheet. In Plate B6 across the sheet (along Z, at  $Z \sim 0$ ) and at some distance along it (along X at  $Z \sim (\pm)$  half-width of the current sheet) the neighbor helicity maximums have opposite signs. Namely that leads to registration of loops in magnetic field hodograms on virtual satellite, as one can see on the left panel in Figure 10. One full loop in the hodogram is seen only if the virtual satellite orbit crosses two vortices with opposite helicities, as shown by the orbit traces in Plate B6 and Figure 10. A trace along diagonal of Plate B6 (crossing two maximum with the same

polarities) would result in ‘S-shaped’ hodograms (see e.g. [Dubinin *et al.*, 2002]). Sliding along X - axis close to the plane with  $Z \sim 0$  provides appearance of multiple loops in the data. On the other hand, the case from Polar (Figure 8) could be also accounted by 3D vortex, similar to the simulated vortices in [Buechner *et al.*, 1998]. Note also that crossing of a single 2D vortex would be seen on a satellite as a part (maximum half) of a loop in the hodogram.

Finally, we compare the experimental  $B_x$  (Plate B4) and model  $B_z$  (Plate B5) bi-spectrograms, the GSE X direction at the MP being the nearest to the current sheet normal, as the model Z axis is. The presence of two sets of horizontal maximums in  $f_L$  constitutes the general similarity in the bi-spectrograms. In the model the lower maximum infers synchronization of the nonlinear (presumably 3-wave) processes inside the reconnected current sheet at the nonlinear state; similar cascade-like synchronization at the higher frequency (upper horizontal maximum) relays with the individual vortex-like structure (single helicity maximum in Plate B6). The third (higher) maximum in  $f_L$  is also visible on both Plates B4 and B5. Similar to the model lower frequency maximum in  $f_L$  in Plate B5, the experimental one in Plate B4 coincide with the low-frequency edge of the spectral slope of  $\sim -1$  in Figure 7. We attribute this maximum to the large-scale wave structures, which synchronize TBL processes globally. As MSH flows interact with MP, which has gradients in its normal direction much sharper than in the parallel ones, those larger-scale waves should resemble the surface ones [Savin *et al.*, 2001, 2002a,b]. Thus, the model data are rather similar to ones discussed above (Plate B4): (i) while the magnetic field transitions in Plate B7 might seem to be independent, they look to synchronize a number of 3-wave processes inside (the similarity in the lower frequency maximums in Plates B4 and B5); (ii) the quasi-coherent structures have the decay-like nonlinear phase-coupling both with global structures (e.g. reconnection sites or ‘magnetic islands’, i.e. the model O-lines) and with the higher frequencies.

In spite of complicated time-dependent geometry (as compared with the plane quasi-stationary one in the model), sharp density gradients in the TBL, limitations in the model grid size etc., we have shown, that the substantial number of the features of TBL turbulence at higher frequencies ( $> 10$  mHz) can be understood by comparison of the experimental data with the model of kinetic current sheet at the nonlinear state. Probably, the evolution of nonlinear structures in the hot inhomogeneous plasma weakly depends on the initial disturbances after exceeding of some amplitude or scale thresholds. E.g., [Chmyrev *et al.*, 1988] have shown that after thinning to the ion gyroradius scale current sheets tend to split into the vortex streets as this state has lower energy as compared with the homogeneous planar current sheet. The characteristic scales of the TBL turbulence are shown to reach the scales of few km, i.e. several electron inertial lengths  $c/\omega_{pe}$  [Savin *et al.*, 1998]. This infers violation of the frozen-in field condition and could be also treated as a feature of the local reconnection near the cusp. The operation of the bursty reconnection for the locally anti-parallel fields over the cusp is in agreement with a number of studies, and the experimental evidences for the permanent by-product reconnection of the TBL strongly fluctuating fields are seen as well (see e.g. [Savin *et al.*, 1998, 2001, 2002a,b, Merka *et al.*, 2000, Onsager *et al.*, 2001, Dubinin *et al.*, 2002]). Thus we could regard the quasi-coherent structures as residuals of the nonlinear evolution of current sheets, the ‘diamagnetic bubble’ presence supports this suggestion as the field depletions in the middle of equilibrium current sheets is wide accepted and a number of modelings predict the small-scale depletions at nonlinear current states (see e.g. [Buechner *et al.*, 1998, La Belle-Hamer *et al.*, 1995]). As a result of the multi-scale reconnection, field lines are connected through the TBL in statistical sense, without opportunity to trace individual field lines in the inhomogeneous non-equilibrium 2-phase medium, one phase being the frozen-in ‘MHD’ plasma another one representing by unmagnetized DB, embedded in the nonlinear current sheets and magnetic vortices. The latter ‘phase’ (in the statistical sense) provides the power-law spectra with the slope  $\sim -1$  (see Figure 7), that implies a special type of translation symmetry of the fluctuations. The quasi-coherent solitons are breaking the Gaussian statistics, most probably due to the TBL intermittency; the mentioned above spectral slope of  $\sim -1$  is consistent with this suggestion.

## 4.6 ACCELERATED PARTICLES

Recent multi-satellite observations demonstrate that the cusp is a locus of accelerated plasma. There is an evidence that cusp is a substantial source of energetic particles (Chen et al., 1997, Chen et al., 1998, Fritz et al., 2000). The energizing is related to the strong turbulence (Chen and Fritz, 1998, Blecki et al., 1999, Savin et al., 2002c), which recently have been mapped by Interball-1 (see above). The ions with energies over 7 keV on June 19, 1998 are seen after 08:50 UT on the spectrograms on panel h in Plate A6. As we've mentioned above, waves in 2-50 mHz range (panels i-k, Plate A6) correlate with intensity of energetic protons (panel h, black line) upstream MP starting from ~08:53 UT; main wave bursts have counterpart in energetic electrons (panel g, black line). Turning now to spectrograms on panels l-m (Plate A6), one could see that the upstream ions correlate best with the  $W_{kin}$ -fluctuations (excluding wide-band spikes on panel j), the maximum energy yellow-colored fluxes at 09:20-09:50 UT exceeds that of the trapped particles under MP. Note also the maximum intensity of the energetic ions just inside MP (i.e. in the 'deepest' PB with ion beta up to 15) with the ion intensity being gradually diminished inside magnetosphere, it is better seen on panel m. The further magnetospheric ion intensifications generally correspond to the  $|B|$  drops (panel d) and dBx bursts (black line on panel i). Thus for rather stationary SW input (panels a, c, d, Plate A6), the soft energetic ions < 100 keV can either leak from magnetosphere due to diffusion by the strong waves or be an extension of the suprathermal tails, accelerated by the higher frequency waves (cf. Savin et al., 1998, 2002c). The higher energy ions infer a local acceleration correlating with the upstream TBL fluctuations. The electron spectra on panel n (Plate A6) upstream MP also generally conform the intensification of fluctuations in  $W_{kin}$ , the electrons up to 50 keV appear. The energetic particle cumulating in PB just under MP can result both from the local cascading of the chaotic kinetic energy and from loosing of parallel momentum by the magnetospheric trapped particles in wave-particle interaction, the latter also is necessary to trap the locally-born accelerated particles in PB. In Plate B8 we blow-up electron and ion energy spectrograms from June 19, 1998 (Plate A6) at 09:30-10:10 UT, adding respective pitch-angles (scales in degrees on the right side). Before 09:47 UT (i.e. in MSH) electrons (panel b) and higher energy ions (panel c) tend to have minimum in field-aligned ions that excludes reconnection as a source for the higher energy ions, as in the southern hemisphere the magnetospheric field is pointed away from the Earth, thus particles, escaping from magnetosphere, should flow parallel to reconnected lines (see details below and in [Savin et al., 1998, 2003b]). The only field-aligned electron burst at 09:48 UT also demonstrates dominating anti-parallel flow (panel b). The main ion maximum upstream MP at pitch angles ~ 90 degrees spreads till high energies that strongly infers a local source for the most dense suprathermal ions. At 09:55-10:05 UT the higher energy ions (> 7 keV) on bottom panel in Plate B8 are peaked at ~ 90 degrees along with the core MSH-like ones. Their fluxes along the field are smaller than the perpendicular ones, but they exceed the anti-parallel fluxes. The latter might imply either providing of a minor amount of the plasma-sheet-like (PS) ions along the field from inner magnetosphere or represents the loss-cone towards the nearest (southern) ionosphere.

On panel a in Plate B8 we blow up panel l of Plate A6 and super-impose the pitch angle. Around 09:40 UT soft ions with energies < 50 keV display minimum along the magnetic field, similar to that of panel c. It gives an estimate for the upper limit of supra-thermal ions of the MSH origin. At higher energy (up to 400 keV) the parallel ion flows dominate that of anti-parallel, that conforms their leaking from PB along effectively reconnected field lines. Further support for that one can found on bottom panel of Figure 11: both intensity and slope of the PB ions at energies > 250 keV coincide in PB (curve 1 marked by full large circles) and TBL (curve 2 marked by full large circles). An instant field-aligned spectrum in TBL (curve b marked by small open circles on bottom panel) from the time interval 09:40:37-09:42:02 UT even better reproduce the average shape of the PB spectrum (curve 3), having slightly smaller intensity. Coming back to panel a in Plate B8, around 09:40 UT there also

## Energetic Ion Spectra on June 19, 1998 DOK-2 (Interball-1)

- 1 - in the Magnetosheath at 09:06-09:12 UT
- 2 - in the Magnetosheath close to the Magnetopause at 09:35 - 09:41 UT
- 3 - Inside the Magnetopause at 09:52-09:58 UT

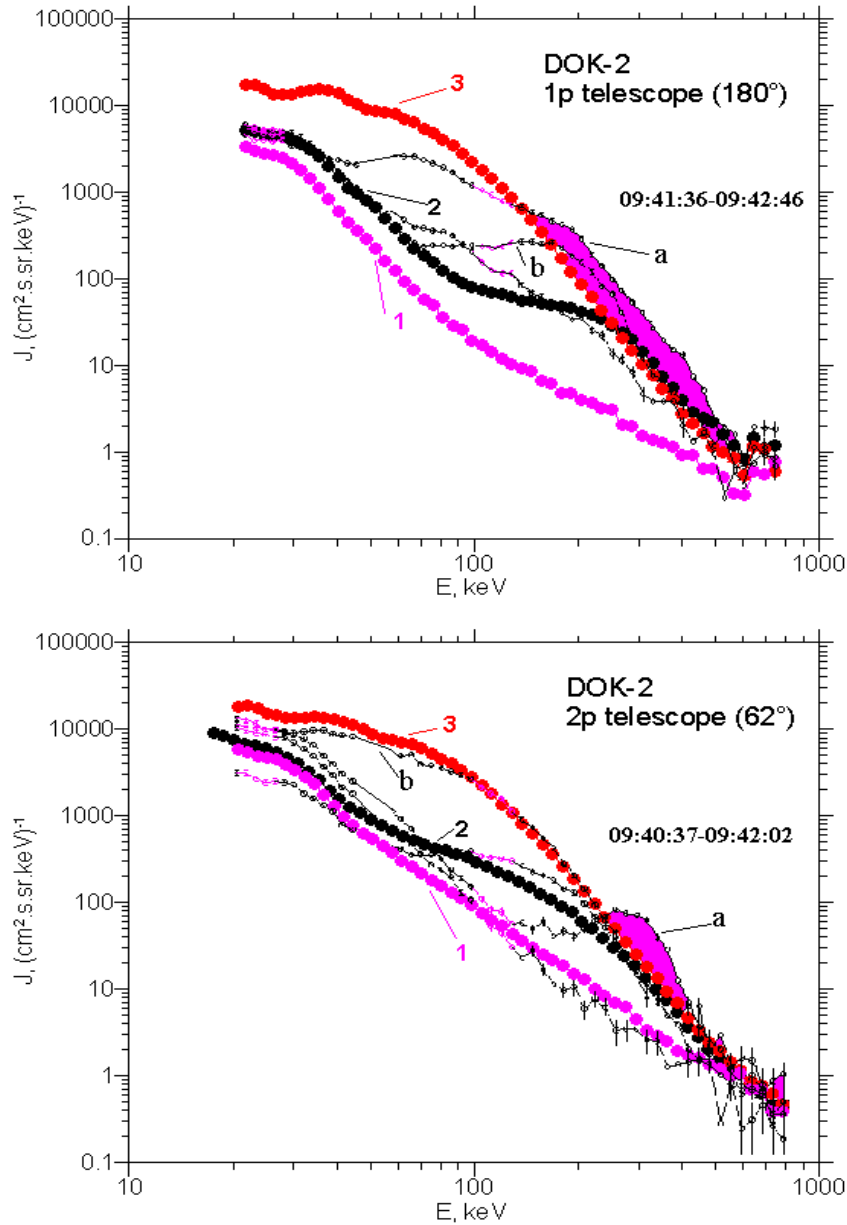


*Fig.11. Energy spectra on June 19, 1998 for tailward (top, FOV 180 degrees from Sun) and sunward (bottom, FOV 62 degrees from Sun) flowing energetic ions; thick circles: 1 – MSH 09:06-09:12 UT, 2 – TBL 09:35-09:41 UT, 3 – PB 09:52-09:58 UT. Small thin circles: top – 09:41:36-09:42:46 UT, bottom – 09:40:37-09:42:02 UT. Shadowing marks difference between average PB and maximum from the displayed spectra in TBL (denoted by ‘a’).*

narrow perpendicular spikes at the higher energy, which constitute the third population of energetic particles in the upstream TBL. Without the parallel speed these ions can result e.g. from the local perpendicular ion-cyclotron acceleration. The characteristic energy spectra are marked in Figure 11 by letters a and b on top panel and by letter a on bottom panel, the difference

between maximal spectra (a) and that of PB (curves 3) is highlighted by shadowing. It reaches factor 3, the spectral shape is representative on top panel (this channel doesn't rotate and has nearly constant pitch angle during exposition of spectrum 'a'). Comparison with panel a in Plate B8 infers that the highlighted spectral difference is the systematic one. Even average spectrum in TBL (2, top panel in Figure 11) is slightly larger than that of PB (3) at energies > 250 keV. Panel a in Plate B8 in PB at 09:53-10:05 UT demonstrates loss-cones anti-parallel magnetic field (cf. panel c); after 10:05 UT the trapped perpendicular component (pitch angles ~ 90 degrees) is seen, having less energy spread compared with that of MSH around 09:40 UT.

On bottom panel in Plate B7 we present color-coded (see logarithmic scale for the count rate on right side) spectrogram of energy per charge (logarithmic scale in keV/e is shown on left vertical axis) for the unique MSH constituent He<sup>++</sup>. It clearly demonstrates the local acceleration of He<sup>++</sup> up to 100 keV/e in the region of numerous plasma jets and MP-like transition at 10-11 UT (see the upper panels and discussion above). Another peculiarity is much greater intensity compared with the MSH stagnation region after 11:30 UT. As for more energetic particles (not shown), the acceleration of ions till several hundreds keV and of electrons till several tens keV is seen namely in TBL with maximum at the multiple  $B_y$  transitions (~10:20-11:10 UT). Note also the difference with Interball: no enhanced energetic particle fluxes inside MP are registered by Polar. Similar case in a stagnation region on April 21, 1996 from Interball-1 data has been described by Savin et al. (2002c). The electrons with energies up to 10 keV can be accelerated by whistler-like fluctuations of about 1 Hz (see Savin et al., 1998). Another case of the open cusp throat is presented in Plate B9. Top panel depicts  $|B|$  (yellow shadowed, scale in nT on left axis) and soft energetic ions (> 30 Hz, logarithmic scale for counts/s on right side) from the same channels as shown on panels l-m in Plate A6 (the 180 degrees channel is marked by black line) during outbound MP crossing on April 15, 1999 (at ~ 17:45 UT). The large-scale  $|B|$  depletion is green-shadowed, it looks similar to PB in Plate A6, but in this case the energetic ion intensities conform the particle source in MSH rather than in magnetosphere: the anti-sunward flowing ions (red line) have greater level in MSH than under MP and dominate over that of sunward one. So similar to Plate B7, we attribute the magnetic field depletion at tilt ~20 degrees to the open cusp throat. Both energetic ions and electrons (bottom panel) have clear strong maximums in the OT and just upstream it, that represents a feature of local particle origin and/or accumulation.

So, we would like to mark 3 populations of energetic particles in the disturbed TBL outside MP:

- dense low-energy heated MSH particles (< 50 keV), they constitute a source for the soft energetic ions in PB (see the dominance of anti-parallel flows on panel a in Plate B8 at ~ 09:40 UT);
- intermediate energy particles escaping from PB inside MP;
- bursty higher energy perpendicular ions, presumably locally accelerated by e.g. ion-cyclotron mechanism in the wide-band developed turbulence.

## 5 STATISTICS FOR PLASMA BALLS AND OPEN CUSP THROATS

After presentation of the Interball-1 and Polar data on June 19, 1998 we would like to return to the largest scale nonlinear sites in the outer cusp – 'plasma balls'. Figure 7 and Plates A6 and B7 demonstrate that at sunward and anti-sunward tilt (i.e. from Polar and Interball-1 data) the MSH flow interaction includes similar features, e.g. characteristic kinked power spectra, accelerated plasma jets and stagnant heated MSH plasma at the MSH-cusp transition. The general difference is that at the positive (sunward) tilts this stagnant plasma locates outside MP (as Figure 1 and Plate B7 infer), while the PB in Plate A6 is certainly inside it (see also Savin et al., 2002a). It means that the cusp throat can be open for direct interaction with MSH flows or closed by MP, depending presumably on the tilt sign. Thus, instead of Figure 1b one might have asymmetric streamlining of the MSH flow around cusps, as shown in Plate B10 (Interball-1 and Polar traces

from Plates A6 and B7 are marked by thick black lines): in the summer (positive tilt) hemisphere MSH flow produce TBL interacting with the MP indentation over cusp; in winter (bottom) TBL locates both upstream MP and at the outer PB border, while the MP indentation might exist it is not so deep as the summer one.

Savin et al. (2003b) demonstrated PB encounters on 4 consecutive Interball-1 orbits on June 15-27, 1998. So, the PB can be rather permanent phenomenon. We use the same full Interball-1 database as for Plates A1 and A2 to explore how characteristic the PB are. In most high-shear cases and when energetic particles mark the clear trapped boundary as in Plate A6, we recognize the PB from key parameters and from energy-time spectrograms of the thermal particles, using the characteristic features discussed above. For ~ 30% of more complicated cases (from 52 PB in Plates A3, A4 and 37 magnetic field cavities with heated plasma in the open OT in Plate A4) we have analyzed the pitch-angle particle distributions (cf. Plate B8) or detailed IMF data. We set the lower duration limit for the large-scale PB at 10 minutes, the smaller 'diamagnetic bubbles' has been studied earlier using high-resolution magnetic field only [Romanov et al., 1999, Savin et al., 1998, 2002a]. In Plate A3 we present distribution of PB in three GSM projections. Gray color marks the TBL encounters with the threshold for  $B_x$ -variation  $> 3$  nT, that demonstrates rather dense Interball-1 coverage of near-MP region (see Plates A1 and A2 and discussions above). Most of PB are concentrated over the cusp throats at negative tilts (blue lines). They tend to occur at the outer TBL border (farther  $\sim 8 R_E$ , that is better seen in Northern hemisphere) and have maximum spread in Y direction. Some of them are registered in the near tail, including most of that at positive tilts (red lines). The spread in the X direction is presumably due to different SW dynamic pressures: e.g. the closest to Sun blue line at  $X > 10 R_E$  corresponds to the case on May 11, 1999, when SW almost disappeared, its size of  $\sim 2.5 R_E$  provides a proxy for the upper limit in X direction. A reasonable estimate for the average PB size from Plate A3 would be  $1-4 R_E$ , the Y-size could be over  $5 R_E$ . The PB width, inferred by [Savin et al., 2002a] for June 19, 1998, is close to the upper limit. For February 18-19, 1997 with very stable SW conditions [Romanov et al., 1999] an estimate for the PB spread along the orbit from satellite- subsatellite time lag is over  $2 R_E$ . Taking into account average MP speed of  $\sim 20$  km/s (versus 1.5 km/s for the spacecraft one), we can accept the average PB scale being closer to the upper limit of its geometrical size in Plate A3.

PB has been identified as |B| large- scale depletions with newly heated plasma inside MP [Savin et al., 2002a]. Before applying the GDCF, the PB had been placed outside MP similar to the stagnation region registered at the beginning of Interball-1 operation [Savin et al., 1998]. We have found 37 cases of the latter type, which resemble Plate B9, i.e. have clear magnetic field, energetic particle behavior or particle pitch- angle features of MSH (cf. Plate B8 at  $\sim 09:40$  UT). The general difference of these cases from PB is that MP, while being imbedded into strong perturbations, effectively isolates the MSH electrons and most of ions from magnetosphere (cf. [Savin et al., 1998]). Another difference is that at the PB outer border the fluctuations, generated in the process of the MSH kinetic energy dissipation (see Plate A6 and respective discussion above), are combined with that at the MP per se (separated in the case of open OT). It enlarges the fluctuation level and, consequently, enforces turbulent transport processes. The tilt dependence of the occurrence of PB (identified in total amount of 52) and open OT, resembled PB in |B| behavior (37 events), is presented in Plate A4. Blue bars mark the number of PB in a dipole tilt interval, red ones – stagnant MSH sited outside MP with large-scale |B| depletions. The green bars denote numbers of PB, for which their being inside MP is supported by energetic particle data (see Plate A6 and related discussion above); black ones – depict number of the external |B|- depletions with clear dominating of the soft energetic particles from MSH. Note, that in  $\sim 15\%$  cases the soft-energetic particle data were absent and that, if the trapped energetic particles have been seen just under MP, their intensity usually exceeded that of MSH ones. Another reason for the weaker energetic particle occurrence in the open OT could be the particle leakage into downflow MSH, while in PB they are returned back by reflecting from the

convergent magnetic field over ionosphere (excluding narrow loss-cones, see Plate B8).

In total Plate A4 conforms the open OT encountering at positive tilts and that of PB at negative tilts: (i) the maximum of 20 PB cases occurs for tilts between -15 and -25 degrees, 77% PB are registered at tilts  $< -5$ ; (ii) 6 open OT are seen at negative and 21 at positive tilts ( $> |5|$  degrees). The energetic particle data prove the PB closed topology in majority of the cases (e.g. in 63% for tilts between -15 and -25 degrees). No clear dependence of the PB occurrence on the magnetic shear across MP has been found, while for  $> 65\%$  IMF  $B_z > 0$ . Savin et al., (2003b) estimated the probability of the PB crossing at GSM  $|Z| > 4 R_E$  at tilts from -15 to -25 degrees being  $\sim 35\%$ , for tilts  $< -5$  degrees  $\sim 25\%$ . Thus, the PB are present rather regularly in the outer cusp at the negative tilts.

The high-beta (2-15) and direct interaction with the incident MSH flows differ PB from the rest outer cusp. Generally in the outer cusp quasi-perpendicular MSH ions are strongly guided by magnetic field (Kirpichev et al., 1999). E.g. on April 21, 1996 [Savin et al., 1998] such ions are registered for ion beta  $\sim 0.4$ . Dominating of PB during IMF  $B_z > 0$  can be accounted for: (i) during southern IMF the minimum  $|B|$  in outer cusp is shifts equatorward that favors penetration of MSH flows into the cusp throat; (ii) drift, caused by inductive electric field from MSH, moves plasma from PB towards plasma sheet for  $B_z < 0$  and from the boundary layer in tail towards PB for  $B_z > 0$ . Quasi-perpendicular ions, visible till the upper energy limit in Plate B8, and electrons are trapped in the diamagnetic cavity. We infer their local heating by the strong turbulence (see e.g. [Savin et al., 1998]) both from continues ion distributions (from the MSH energies till the soft energetic particle ones) and from their absence outside PB deeper in magnetosphere. Particles from plasma sheet also can contribute into the trapped population (Shabanski and Antonova, 1968), but for that they should loose their parallel momentum by the wave-particle interactions.

## 6 DISCUSSION

After the presentation of two characteristic cases from Inteball-1 and other ISTP spacecraft data and statistical study of perturbations near high-latitude MP we would like to discuss the presented and earlier published data from this region. The previous results and respective references the reader can find in [Savin et al. (1998, 2001, 2002a,b, 2003a,b)].

### 6.1 TURBULENT BOUNDARY LAYER GENERAL PROPERTIES

An inspection of the TBL crossings by Interball-1 (Plates A1-A3) shows that on January 27, 1997 and on June 19, 1998 the TBL is registered at rather usual positions (see sections 2, 4). Both case and statistical studies show that the interaction of MSH flows with the high latitude MP is neither smooth nor laminar. The interaction produces a layer with strong nonlinear turbulence – the TBL. TBL concentrates at high latitudes ( $|Z| > 4 R_E$ ) over cusp and downstream it, maximizing along the transition region from the mantle to the low latitude boundary layer (see Plates A1-A2). The TBL 'wings' range from the near-cusp TBL into the tail down to  $X \sim -20 R_E$ . Savin et al. (2002a) have demonstrated that a substantial part of the events in those 'wings' at the higher latitudes is independent on the interplanetary (IMF)  $B_y$ , which contradicts the 'sash' predictions.

Approximately another half of the 'wing' events follows the 'sash'  $B_y$ -dependence. Another possible 'wing' source is the TBL downstream cusps (see Figures 1, 3 and related discussions). The TBL is present in  $> 80\%$  of the high-latitude MP crossings. The most intense events could be approximated by the effective disk with diameter of  $6 R_E$  above the dayside cusps with an average maximum RMS of about 22 nT (see Savin et al., 1999). At low latitudes the intensive events are encountered mostly in the tail. The northern TBL is indented in the YZ- plane, the events with positive and zero tilts dominate (Plate A2). It conforms the direct interaction of the open cusp throat with the incident MSH flows (Figure 1). In such cases the tailward wall of cusp

throat represents the rising obstacle for the flow, similar to the gas dynamics case (cf. Haerendel, 1978). The indentation in TBL/MP does not represent a characteristic feature of the winter hemisphere, TBL events with negative tilts strongly dominate near  $Y \sim 0$  at negative  $Z$  (Plate A2). This asymmetry suggests that the interaction of the MSH flow is different for the negative and positive tilts (see Plate B10). No such crucial dependence had been found for the IMF direction, while specific shifts has been outlined e.g. by Merka *et al.*, (1999).

Essential MSH plasma heating ( $\sim 300$  eV) occurs in 82 % of the cases within the TBL ‘magnetic bubbles’ (see Figure 3 and deep spiky depletions of  $|\mathbf{B}|$  in Plate B7). The magnetic field in the ‘bubbles’ is highly reduced ( $>8$  times on average). The TBL ‘wings’, visible also in the ‘diamagnetic bubble’s distribution, indicate the possibility of MSH plasma penetration into a wider region than just over the dayside cusps (cf. Haerendel *et al.*, 1978, Savin *et al.*, 1999, 2003a, Romanov *et al.*, 1999).

The correlation of soft energetic particles with the strong turbulence (see section 4.6 and Chen and Fritz, 1998, Blecki *et al.*, 1999, Savin *et al.*, 2002c) has been confirmed by the Interball-1 and Polar data on June 19, 1998. The energetic particle presence also helps in placing of PB and open OT inside or outside MP (see section 6.3 below). Detailed pitch-angle distributions and energy cuts point on 3 populations of energetic particles in the disturbed TBL outside MP:

- dense low-energy heated MSH particles ( $< 50$  keV), they constitute a source for the soft energetic ions in PB (see panel a in Plate B8);
- intermediate energy particles escaping from PB inside MP;
- bursty higher energy perpendicular ions, presumably locally accelerated by the wide-band developed turbulence.

In PB the loss-cones in ion distributions with energies  $> 7$  keV towards the nearest (southern) ionosphere conform PB being a source for precipitating particles in the dayside cusp ionosphere.

## 6.2 MULTISCALE RECONNECTION

On June 19, 1998, the data display typical TBL features (Plates A6 and B7): wideband intensive nonlinear fluctuations (with energy density up to 45% of kinetic plasma energy density in flowing MSH), ‘diamagnetic bubbles’ with  $|\mathbf{B}|$  drops from  $\sim 75$  nT down to few nT (Plate B7), plasma heating and nearly Alfvénic field-aligned jets etc. (cf. Savin *et al.*, 1998, 2002a,b, Sandahl *et al.*, 2000). The latter has been accounted for reconnection bulges at the border of the outer cusp (Dubinin *et al.*, 2002, Khotyaintsev *et al.*, 2003). To combine that with well-known reconnection at northward IMF downstream the cusp for smooth MP, we propose the scheme depicted in Figure 12a: on the indented MP in the open cusp throat (cf. Figure 1b, Plate B10) there are at list two places with anti-parallel magnetic field on the MP. The upper reconnection site is the ‘standard’ large-scale tail reconnection, the lower one is inside OT superimposed on the TBL fluctuations. The original magnetospheric field lines are marked by the lines with arrows, and those of the IMF by ones with circles. Reconnection pulses inside OT can be recognized in Plate B7: the local magnetic field is practically anti-parallel (see changes in  $B_y$ ), the dominant positive  $V_y$ -bursts correspond to the predicted by reconnection magnetic stress, accelerating the MSH plasma (Dubinin *et al.*, 2002). However, comparison with the SW data from Geotail via GDCF obviously demonstrates no evidence for the SW driving of the plasma jets. Instead, the jets repetition conforms TBL- driving (see Figure 7 and related discussions above). Savin *et al.* (2002a) accounted for the difference of the power for Polar and Interball spectra in Figure 7 of about one order of magnitude by the average magnetic field annihilation in the patchy reconnection. Similar reasoning for May 29, 1996 has been proposed by Savin *et al.* (2003a). Simultaneously, Plate B7 demonstrates strong prevailing of the jet kinetic energy over the magnetic one, that invokes the reconnection triggering by the accelerated plasma jets at the TBL outer border (see Plate A6, Figure 5 and related discussions). This bursty reconnection corresponds to the smaller (middle) scales. Later on we refer to this as ‘primary cusp reconnection’. Its characteristic scale is estimated as 1000-2000 km (Savin *et al.*, 2002a).

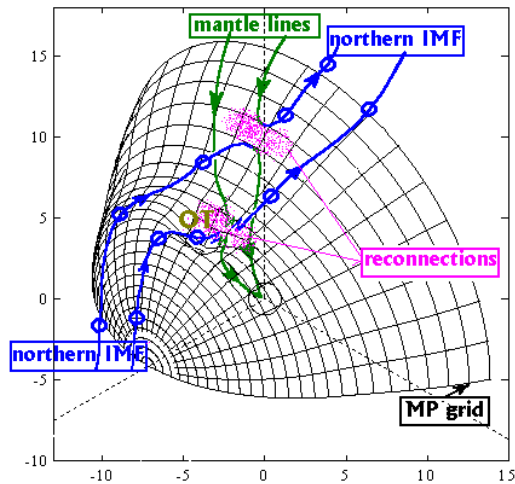


*Fig. 12a. Sketch for multiple reconnection sites at the indented MP for the northern IMF*

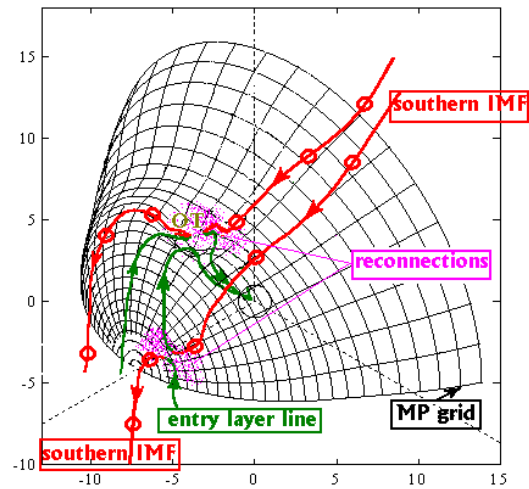


*Fig. 12b. Sketch for multiple reconnection sites at the indented MP for the southern IMF*

Figure 12b gives the respective picture for the southern IMF (cf. Savin *et al.*, 2002a). Now the ‘classic’ large-scale reconnection is shown at the bottom. Savin *et al.*, (2003a) demonstrate parallel operation of the ‘classic’ remote laminar reconnection tailward the cusp on May 29, 1996 for dominant IMF  $B_z > 0$ .

We reproduce in Figure 13 the Magion-4 data on vertical/sunward ion flows (Savin *et al.*, 2002a). Especially suggestive for the local reconnection are the sunward/vertical flows in the cusp vicinity during negative IMF  $B_z$ . We would like to outline that events with  $B_z > 0$  do not concentrate exclusively at the high latitudes nor do the events with  $B_z < 0$  tend to be at the low latitude cusp border. Such shifts are anticipated when the stretched by the MSH flow field lines are situated along the indent MP in the cusp vicinity. This is schematically shown for negative  $B_z$  in Figure 12b, where in general the MP nearly anti-parallel fields will be nearer the equator and at the equatorial cusp border (see also Figure 12a for the northward IMF). Thus, one expects favorable for the reconnection situation at these places, both of which map to the cusp equatorial border in the ionosphere. Figure 13 implies the parallel operation of the reconnection for the locally anti-parallel fields over the cusp (middle scales), along with the by-product reconnection of the TBL strongly fluctuating fields (small scales  $\sim$  ion gyroradius, see e.g. Savin *et al.*, 2002a,b, Merka *et al.*, 2000, Fedorov *et al.*, 2000). We would like to note also that, as can be seen from the Figure 12, the remote from cusp reconnection can take place independently. Belmont and Rezeau (2001) developed a linear theory which predicts that strong ULF fluctuations that occur just outside of or at the magnetopause can independently result in micro-reconnection and local plasma penetration all along the magnetopause surface even in the absence of quasi-stationary macro-reconnection of anti-parallel magnetic fields. Another possibility is that secondary reconnection of the fluctuating fields in the TBL (regardless of the origin of the TBL) can provide the plasma inflow in the quasi-parallel case. This reasoning is along the lines of the Haerendel (1978) predictions and findings of Savin *et al.* (1998b) for other IMF directions. The reconnection bursts can provide a particular mechanism for the effective ‘interconnection of the parallel fields’ (see Chandler *et al.*, 1999 and references therein).

Summarizing the discussion above, we suggest that multiple reconnection sites might operate simultaneously:

- Remote (from the cusp) reconnection site that is predicted by the MHD model (Fedder *et al.*, 1995), the scale of the coherent flow pattern can be evaluated up to a few earth radii;
- Primary cusp reconnection site(s) at the location of the anti-parallel average fields (of  $\sim$  few thousand km), where local magnetic field annihilation enforces the fluctuation level and heating;
- Secondary (by-product) reconnections of the highly fluctuating fields potentially at all locations within the TBL, that can occur at small scales (down to an ion gyroradius) even for the low-shear average fields (cf. Haerendel 1978, Savin *et al.*, 1998 and Chandler *et al.*, 1999).

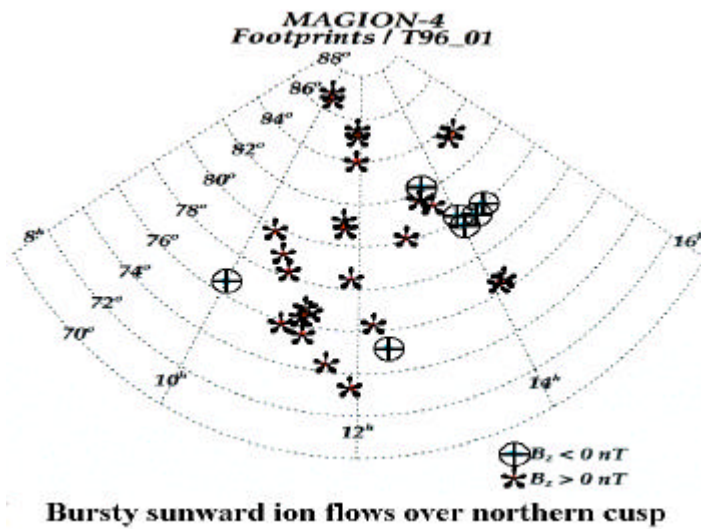


Fig. 13. Ionospheric projections of the exterior cusp reconnections (Savin et al., 2002a)

The micro-reconnection creates the specific structure of the MP current sheet(s) with magnetic islands, which results in plasma percolation through the non-linear boundary network (Kuznetsova and Zelenyi, 1990). The order-of-magnitude estimate shows that this stochastic plasma transfer through the TBL/cusp walls might provide a means of populating both the cusp and low latitude boundary layer (LLBL): the diffusion coefficient  $D_p \sim (5-10) 10^9 \text{ m}^2/\text{s}$  for typical MP parameters results in a particle influx of  $(1-2) 10^{27}$  particles/s (Savin et al., 1999). Primary cusp reconnection should certainly amplify the plasma inflow.

Comparison with the kinetic simulation of thin current sheets (see section 4.5 and Savin et al., 2002b) demonstrates reproducing of general polarization, spectral and bi-spectral properties of the TBL fluctuations by the modeling. E.g. the registered quasi-coherent structures can be regarded as residuals of the nonlinear evolution of the thin current sheets; the ‘diamagnetic bubble’ presence supports this suggestion as the field depletions in the middle of equilibrium current sheets is reproduced by a number of modeling of the nonlinear current states (see e.g. [Buechner et al., 1998, La Belle-Hamer et al., 1995]). As a result of the multi-scale reconnection, field lines are connected through the TBL in statistical sense, without opportunity to trace individual field lines in the inhomogeneous non-equilibrium 2-phase medium, one phase being the frozen-in ‘MHD’ plasma another one representing by unmagnetized ‘diamagnetic bubbles’, embedded in the nonlinear current sheets and magnetic vortices. The latter ‘phase’ (in the statistical sense) provides the power-law spectra with the slope  $\sim -1$  (see Figure 7), that implies a special type of translation symmetry of the fluctuations. The quasi-coherent wave-packets are breaking the Gaussian statistics, most probably due to the TBL intermittency; the mentioned above spectral slope of  $\sim -1$  is consistent with this suggestion.

### 6.3 PERTURBATION OF MAGNETOSHEATH FLOWS BY THE OUTER CUSP THROAT

Now we would like to address another primary mechanism for the energy and mass transfer at the MSH/cusp interface: the direct interaction of the MSH flow with the outer cusp throat (OT). From Figure 1 and Plates A1-A3, A6 and B7-B10 we see that the cusp throat might present a substantial obstacle for the plasma flow streaming around the MP. While the magnetic topology of the throat occurred to depend on the dipole tilt angle, the general consequence for the incident MSH flow in a self-consistent regime is that the flow interacts at high latitude with pre-existed high-beta stagnant plasma instead of the magnetic barrier at low latitudes (cf. Lavraud et al., 2002). In the zero approximation the magnetic barrier can be regarded as a ‘rigid’ quasi-stationary current sheet, the

large-scale laminar reconnection being inferred as the primary mechanism for the mass and energy transfer inside MP (see e.g. Russell (1995) and references therein). For the plasma-plasma interaction in high-beta regime over cusp throat neither magnetic pressure nor magnetic stress could stop/deflect or accelerate the incident MSH flow. Thus, only high-amplitude waves and, probably, surface charge at MP can constitute the means for the interaction.

Multi-point data on January 27, 1997 permit not only to evaluate the TBL depth in the near tail as being  $\sim 2 R_E$  from the satellite-satellite measurement comparisons (see Figure 3 and related discussions in section 2). The difference of this case from the rest discussed ones is that Interball-1 traces cusp and then goes downstream the cusp, while the rest ones deal with transition from the OT/stagnation region towards the Sun, i.e. upstream into the unperturbed MSH flow. Its provide an opportunity to get the quantitative estimate for the drop of the kinetic energy density,  $E_k$  (relative to the thermal one,  $E_t$ ) due to the MSH flow interactions with the tailward cusp wall. The high latitude TBL might result in the substantial MSH kinetic energy transformation into the thermal one (from 20 to 50 % of  $E_t$  relative to  $E_t + E_k$ ), the energy re-distribution being visible downstream the tail TBL. That conforms the chaotization of  $\sim 40\%$  ion kinetic energy in the upstream TBL on June 19, 1998 (see sections 4.2 and 6.4). The schematic representation of the resulting picture is show in Plate B10 (upper part). The model of Spreiter and Stahara, 1980 predicts the gain of  $E_k/E_t$  to be  $\sim 2$  for Geotail relative to Interball-1 in Figure 3 at  $\sim 1120$  UT, while the measured gain is  $\sim 8$ , i.e.,  $E_k/E_t$  drops by a factor of  $\sim 4$  at high latitudes in comparison to the simultaneously obtained low latitude values, re-calculated to the same X. Following Haerendel (1978) we address this deceleration to the MSH flow interaction with rising field lines at the tailward wall of the outer cusp throat. The sound Mach number in the unperturbed MSH ( $M_s \sim 2$ ) drops to  $M_s \sim 1$  downstream the cusp obstacle. The Rankine-Hugoniot relations predict the maximal temperature gain  $\sim 1.7$ , say, at 13 UT downstream the TBL. Simultaneous temperature ratio on Interball-1 and Geotail is 2.5-3 (Figure 3, panel d), but after the recalculation for the same X using the model of Spreiter and Stahara (1980) the temperature ratio on two spacecraft becomes 1.5-1.8. It is reasonably close to the Rankine-Hugoniot prediction. Thus, the  $M_s$  supersonic/subsonic transition is compatible with the existence of intermediate/slow shock(s) in the vicinity of the tailward cusp wall (see Figure 1 and Yamauchi and Lundin, 1997). But in the upstream TBL (Figure 3, e.g. at 10:30 UT) the  $T_i$  on Interball-1 is again about twice higher than the downstream value (e.g. at 13 UT). In such situation one might invoke some kind of 'thick' transition, when the distributed TBL perturbations are forming the network through which the MSH plasma percolate (cf. Kuznetsova, and Zelenyi, 1991). The correspondence of the temperature gain in that case to the Rankine-Hugoniot relations is only reflecting the conservation laws, but does not imply obligatory the shock transition. We suggest that strong ion acceleration/heating in the TBL results from the MSH kinetic energy multi-step conversion in the TBL via wave-particle interactions. Comparison with the lower altitudes data in the boundary cusp (Interball-2, Figure 4) and in the 'sash' (Polar, panel i in Figure 3) demonstrates that the TBL heating can't account for the full ion energy gain at low altitudes. The extra acceleration/heating mechanism(s) should be invoked for the ion data interpretation in the lower altitude cusp (cf. Lundin *et al.*, 1991).

Savin *et al.* (1998b) demonstrated that just outside OT on April 21, 1996 on Interball-1 the flow is supersonic with the sound Mach number  $\sim 1.3$ . It indicates that the subsonic streamline over cusps is not probable (cf. Yamauchi and Lundin, 1997) and the high latitude deceleration from the supersonic velocities is operating. But the ion TBL heating in  $\sim 3$  times compared with unperturbed MSH in that case is twice higher than the Rankine-Hugoniot maximum prediction ( $\sim 1.5$ ). That is suggestive for the valuable role of the direct interaction of the incident flow with the TBL structures. For the extra heating in TBL the mechanism can be the by-product small-scale reconnection of the fluctuating fields (cf. Haerendel, 1978). In the OT outside TBL (see Fig. 1) the  $T_i$  rise fits the Rankine-Hugoniot relations on April 21, 1996, i.e. compatible with the shock-like transition from the steaming to the stagnant MSH outside TBL. From the other hand, in the two cases, described in Savin *et al.* (1998b) the MSH/OT transition is going through the thin magnetic barriers with  $E_m$  of about  $E_t + E_k$  in both MSH and OT. The latter doesn't resemble intermediate/slow shock solutions (see e.g. Karimabadi *et al.*, 1995) but it is consistent with the nonlinear

vortex streets (see Figure 6 and Savin *et al.*, 1998, 2001).

$M_s \sim 2$  is also seen in the Interball-1 data just outside the MP on May 29, 1996 (Savin *et al.*, 1998a, 2003a). Savin *et al.* (2001) compared the maximum ion heating in TBL on April 2, 1996 with the Renkin- Hughoniot predictions for shock transitions using magnetosound Mach number ( $\dot{I}_m \sim 1.2$ ) in MSH, Alfvénic one for the normal ion speed ( $\dot{I}_{An} \sim 1.2$ ) upstream OT and full Alfvénic Mach number ( $\dot{I}_A \sim 3.5$ ):  $T_i/T_{MSH} \sim 1 + (\gamma - 1) M^2 \sim 1.6$  and  $\sim 5$ , respectively for the Mach numbers of 1.2 and 3.5; we take  $\gamma \sim 5/3$ , and take into account that  $E_t \gg E_k$  in OT. The experimental ion temperature gain in those day of  $\sim 2.2$  is higher than it should be at the inclined shock transition, but it is still much less than the maximum heating at the perpendicular shock. Thus they concluded, that the energy transformation in TBL significantly differs from the thin shock transition: i.e. the disturbed region at 09:45 – 10:00 UT in Plate A6 should be treated as unique ‘thick’ region with both remotely operated ion velocity and pressure cascades and local discontinuities (e.g. MP and outer TBL boundary at  $\sim 09$  UT). For June 19, 1998 existence of two ion populations (at 09:50-11:30 UT in Plate A6) prevents direct comparison with the Renkin- Hughoniot predictions, while bursty super-Alfvénic flows in the upstream TBL and PB (see discussion of the jet at 09UT in section 4.2 and Figure 3b in Savin *et al.*, 2002a) obviously contradict the MHD descriptions with thin shocks. Thus, we think that the finding of the MSH flow deceleration/heating downstream of the high latitude cusp represents a valuable result that outlines the significance of the bulk flow energy transformation in the process of the flow interaction with the outer cusp throat.

We would like to point out also that the TBL not only regulates the penetration of the ‘remote’ ion flows, but also provides both plasma penetration from the MSH and secondary magnetic flux reconnection. This magnetic flux, reconnected at small scales, on average, is capable of driving magnetospheric convection (Haerendel, 1978). In fact at this point we touch an open critical problem of the SW/magnetosphere interaction: where are the Earth magnetic field lines being opened? Our current understanding is that this process is one of multi-point and multi-scale. We believe that the MSH/cusp interface plays the dominant role at least in quasi-steady conditions.

The tilt angle dependence of the cusp position both at high and low altitudes (Zhou *et al.*, 1999, Merka *et al.*, 1998, Smith and Lockwood, 1996) has a natural explanation if the TBL is a general source of plasma for the cusps: (a) the higher the tilt (i.e. the closer the dipole axis to the Sun), the more open the OT for the external MSH flow (i.e. the OT tailward wall represents the steeper obstacle for the MSH flow); (b) the higher the shift/penetrations at the OT tailward wall, the deeper the MSH plasma will be seen on the tail field lines; (c) the deeper the plasma penetration (and/or tailward field line deflection), the more tailward it will be projected into the polar cap (i.e. the cusp is at higher invariant latitudes). Note that the tilt-related cusp shift has no explanation in the ‘traditional’ global-reconnection approach.

At anti-sunward dipole tilts Interball detects demagnetized heated plasma of MSH origin in ‘plasma balls’ (52 cases), which have scales  $\sim$  few  $R_E$ , on the earth side of the MP. The thick multi-layered structure implies a type of interconnected non-equilibrium boundary, the PB represents a local obstacle (partially absorbing) for the incident MSH flow. The observed high-amplitude waves constitute the means for their interaction. The large-scale PB can have substantial impact on the MSH /magnetosphere interactions as a storage of MSH plasma, which in turn becomes a source of the MSH plasma to the magnetosphere. A sunward tilt opens OT for direct interaction with the MSH flow. The asymmetric streamlining of the MSH flow around cusps is shown in Plate B10: in summer MSH flow produces TBL over outer cusp; in winter TBL locates both upstream MP and at the outer PB border. Most of PB are concentrated over the cusp throats at the outer TBL border and have maximum spread in Y direction. The general difference of the 37 cases with the open OT from PB is that MP, while being imbedded into strong perturbations, effectively isolates the MSH electrons and most of ions from magnetosphere. The energetic particle data prove the PB closed topology in majority of the cases. No clear dependence of the PB occurrence on the magnetic shear across MP has been found, while for  $> 65\%$  IMF  $B_z > 0$ . The probability of the PB crossing at GSM  $|Z| > 4 R_E$  at tilts  $< -5$  degrees is  $\sim 25\%$ . Thus, the PB are present rather regularly in the outer cusp at the negative

tilts and they could provide a valuable contribution in populating of the magnetosphere by MSH plasma and also store soft energetic particles in the minimum- $|B|$  configuration (cf. sections 4.6, 6.1 and *Shabanski and Antonova, 1968*).

#### 6.4 TURBULENCE SOURCES AND PROPERTIES

Following Haerendel (1978), we suppose that first of all the TBL results from the turbulent mixing driven by the regular MSH flow interaction with the deformed near-cusp magnetopause. The disturbed flows, accelerated in a remote from cusp reconnection site, can contribute to the TBL generation as well. Remote reconnection site also regulates the TBL position by shifting the MP indentation according to the SW parameters. Away from the plasma stagnation region in the OT center, the Kelvin-Helmholtz plasma vortices with secondary reconnections should provide a mechanism for plasma heating/transport (cf. *Chen et al., 1998*). The fluctuation level in the MSH, especially downstream of quasi-parallel bow shocks, is believed to stimulate the ULF turbulence generation in the TBL. *Savin et al. (2003a)* reported that the correlation at the time interval of  $\sim 5$ -15 minutes in the post-BS region and middle MSH and in the OT reaches 0.6- 0.7 and it is a manifestation of the TBL/MP reactions to the SW/MSH transients. We have mentioned above in section 4.1 similar correlation between Interball-1, Polar and Geotail in response to an IMF  $B_z$  sign changing. Thus, the transient current sheets and density gradients generated by dynamic SW interactions with the MP should contribute in the TBL energy balance. However, simultaneous Geotail spectra infer inherent character of the main TBL disturbances (Plates A5 and A6, Figure 7). We think that, as a whole, the TBL collects, transforms and generates the plasma flow and magnetic field disturbances simultaneously from several sources. Its status depends on the short-term time history of the SW/magnetosphere interactions, influencing, in turn, the interaction of the magnetosphere with newly-arriving disturbances at each particular moment. The simultaneous Interball/Polar magnetic data demonstrate the presence of a maximum at 1- 2 mHz throughout the TBL in both hemispheres (Figure 7). The spectra of  $W_{kin}$  and  $nT_i$  (Plate A6, Figure 5) allow tracing this disturbance throughout MSH.

Besides the transient/dynamic reactions of the TBL to external disturbances, the TBL appears to have well-defined inherent properties, which we have been fortunate to trace at different points of the MSH and MP boundary layers during the favorable period of relatively steady SW parameters. The modern wavelet technique provides us with strong evidence that the spectral characteristics of the TBL in different hemispheres on June 19, 1998 are well defined. The most pronounced TBL waves at 0.005-0.5 Hz have the characteristic kinked shapes and slopes (Figure 7). We have checked the waves in the TBL on August 26, 1995, May 29, 1996, June 23, 1998 and found that the kinked shape with slopes of 1-1.5 and 2-2.6 are characteristic for the TBL. The higher value of the slope in the TBL of  $\sim 2$  is close to that characteristic for the developed self-consistent kinetic turbulence in the geomagnetic tail (see e.g. *Zelenyi and Milovanov, 1998* and references therein). Comparison with the simulation of thin current sheets provides evidences that the random current sheets with features of coherent wave-packets can result in the slopes of  $\sim -1$  in the magnetic power spectra (see sections 4.5, 6.1 and *Savin et al., 2002b*).

*Savin et al. (2001)* have proposed for the open cusp throat the following self- consistent concept of the TBL interactions. Cascade-like wavelet and bicoherence spectrograms and wavelet correlation time infer coherent, most probably 3-wave, interaction between wave trains, while the disturbances seem to be random in waveforms. The coherent large-scale structures, which organize phase coupling throughout the entire TBL, can result from the inverse cascades of the local wave trains. The local wave trains originate from the interaction of the disturbed MSH flows with the MP, their dispersion is indicative for the kinetic Alfvén waves (KAW, see *Stasiewicz et al., 2000* and *Savin et al., 2003a*). *Johnson and Cheng (1997)* proposed excitation of the transverse KAW at MP by interaction of the compressible MSH waves with the current sheet: the wave properties discussed above are in satisfactory agreement with their predictions. Later *Belmont and Rezeau (2001)* demonstrated the growth of the trapped large-amplitude KAW inside the non-uniform current sheets.

At the nonlinear stage the Alfvénic disturbances in the TBL modulate the incident MSH flow in a self-consistent manner, being globally synchronized by phase coupling with the large-scale variations (at  $\sim 3\text{-}5$  mHz, see Plate A6, Figure 5 and Savin et al., 2003a). Our new finding here from the ion fluctuations is the global over-MSH synchronization at  $\sim 1.3$  mHz, the MSH synchronization is seen mostly in the density fluctuations, which are transformed into the velocity ones in the upstream TBL (Plates B1-B3). Turning back to the TBL interaction scheme, while linear KAW resonances (i.e. singularities in the equations of Belmont and Rezeau, 2001) are absent, we suggest that the coherent large-scale structures can originate from the reverse KAW cascades, focused by the concave MP and/ or cusp walls in the outer cusp vicinity. (cf. Plates A6, B1-B4 and Savin et al., 2001, 2003a). The Alfvénic TBL disturbances in turn modulate the incident MSH flow in a self-consistent manner, being globally organized by the phase coupling with the large-scale variations. Thus, the chain is closed: TBL seems to be ‘thick’ multi-scale self-organized system of interacting nonlinear waves. It infers qualitative difference from the traditional approach when the MSH/cusp interaction is regarded as linear superposition of magnetospheric responses on the solar wind or MSH disturbances. Note also that the long-term correlation is suggestive for the systems out of equilibrium near the critical point (cf. Consolini and Lui, 2000). The kinked TBL spectra with characteristic slopes remarkably resemble that in the near-Earth neutral sheet in the state of the self-organized criticality (see e.g. Zelenyi and Milovanov, 1998). Using  $V_A$  as the proxy for evaluation of the characteristic scale at  $\sim 1.5$  mHz, one gets  $L \sim V_A / f_L \sim 3\text{-}7 R_E$ . It is comparable with the TBL span along MP in the indentation or with that of ‘plasma ball’ (Plate B10). From the other hand, the spectral maximum seen from MSH, through TBL and till outer cusp (see Plate B1 and B2) conforms the global character of the registered phenomenon. Such long waves can pass through the MP (see Plate B2) and might resonate with the dayside flux tubes in the PC 4-5 range or at higher harmonics (cf. Pilipenko *et al.*, 1999).

The presented above general scheme has been defined concretely in section 4.2 for the low-shear MP in front of PB. As we’ve mentioned above, it is valuable both because of different type of the plasma-plasma interaction (versus plasma-magnetic barrier one at low-latitude MP), and because the resulting PB inside MP represents great MSH plasma reservoir for the inner magnetosphere. The main means for the plasma-plasma (i.e. MSH flow with PB) interaction are namely the nonlinear waves in TBL upstream MP in the flowing MSH. It is subtended in the above general scheme, but it has been poorly studied at high latitudes. The main physical problem to address is that practically demagnetized PB (ion beta  $\sim 15$ ) can’t interact with the flow via the magnetic forces, it constitutes the principal difference with the dayside low-latitude MP, which is generally a magnetic barrier. We have analyzed the detailed dynamics of the ion energy and of Poynting flux to clarify the pattern of interactions in the upstream TBL. The wave packets, going upstream MSH flow from MP, occur to stimulate partial randomization of the flow via 3-wave interaction far in front of MP ( $> 1$  hour). The interaction with the upstream waves launches downstream the flow current sheets, which can confine super-Alfvénic tailward jets and ignite the cascade-like nonlinear energy transformation in TBL. The jetting (incompatible with a reconnection) and wave ignition result in the MSH kinetic energy drop by  $\sim 40\%$ , the jet transports downstream the ion momentum excess. The kinetic energy drop results also in amplification if the low-frequency pulsations ( $\sim 1.3$  mHz), three periods of which ( $\sim 15$  minutes) cover the upstream TBL, these fluctuations are phase-coupled with the spectral maximums at 3-10 mHz at  $\sim 09:00, 09:15, 09:30$  and  $09:45$  UT in Plates A6, B1, B2. It conform the ‘thick’ TBL transition invoked by Savin et al. (2001) versus a ‘thin’ shock-like one, i.e. a macro-equilibrium could be not achieved in the outer BL during few its characteristic periods (and, probably, throughout few characteristic wave-lengths). The strong upstream fluctuations in plasma density and velocity can be visible at the lower latitudes as slow mode transitions (Song, 1992).

## 6.5 CONCLUDING REMARKS

The results of our data analysis strongly indicate that the TBL fluctuations, instead of being random, are phase-coupled and 'organized' by the cascades of nonlinear, presumably 3-wave, interactions. The selected coherent wave trains are capable of synchronizing interactions throughout the TBL, somewhat resembling a global TBL resonance. For the 'organizing' wave mode we get 3-4  $R_E$  as a proxy for the characteristic scale. This is close to the diameter of the TBL or outer cusp throat (Plates A1-2) and can be attributed to a standing nonlinear wave, trapped in the outer cusp throat. The quasi-coherent structures control the spectral shape and result in non-Gaussian statistical characteristics of the disturbances, that conforms the fluctuation intermittency.

We suggest that multi-scale TBL processes play at least a comparable role to those of reconnection remote from the cusp in the solar wind energy transformation and population of the magnetosphere by the MSH plasma. The TBL transforms the MSH flow energy including deceleration and heating of the flow downstream the high latitude cusp.

The plasma-plasma interaction over cusp throat operates via reflected waves, which ignite the chaotization of ~ 40% upstream kinetic energy, the sub-Alfvénic flow decay launches the TBL nonlinear cascades along with the downstream jets accelerated up to 3 Alfvénic Mach numbers.

## ACKNOWLEDGMENTS

We thank K. W. Ogilvie and the SWE team for providing WIND solar wind dynamic pressure data, R. Lepping and J. H. King for providing WIND and Imp-8 magnetic field data and J. Scudder for providing the HYDRA data. We thank the GEOTAIL/MGF team, especially Dr. H. Matsui, for providing their high-resolution magnetic field data used in this paper. We appreciate fruitful discussions with G. Haerendel, A. Fedorov, G. Zimbardo, M. Yamauchi, A. Otto, T. E. Moore, T. G. Onsager and R. Lundin along with the help in the paper preparation by A. B. Belikova, I. Dobrovolsky and V. Prokhorenko. Work was partially supported by International Space Science Institution, European Commission Research Training Network HPRN-CT-2001-00314 and by grants, INTAS-2000-465, KBN 8T12E 047 21, RFFR 02-02-17160,

## REFERENCES

- Anderson, R. R., C. C. Harvey, M. M. Hoppe, B. T. Tsurutani, B. T. Eastman, J. Etcheto**, Plasma waves near the magnetopause, *J. Geophys. Res.*, **87**, 2087, (1982).
- Angelopoulos, V., F.S. Mozer, J. Bonnell, M. Temerin, M. Somoza, W.K. Peterson, H.L. Collin, and B. Giles**, Wave power studies of cusp crossings with the Polar satellite, *J. Geophys. Res.*, 106(A4), 5987, (2001)
- Avanov, L.A., V. N. Smirnov, J. H. Waite, Jr., S. A. Fuselier, and O. L. Vaisberg**, High-latitude magnetic reconnection in sub-alfvénic flow: Interball Tail observations on 29 May 1996, *J. Geophys. Res.*, **106**, submitted (2001)
- Belmont, G. and L. Rezeau**, Magnetopause reconnection induced by Hall-MHD fluctuations, *J. Geophys. Res.*, **106** (A6), 10,751-10,760, (2001)
- Belova, E. V., J. Blecki, M. Denis, L. M. Zelenyi, and S. P. Savin**, Excitation of ion cyclotron waves at the boundary of the magnetosphere, *Sov. J. Plasma Phys.*, **17**, 555, (1991)
- Blecki, J., H. Rothkaehl, K. Kossacki et al.**, ULF-ELF-VLF-HF Plasma Wave Observations in the Polar Cusp Onboard High and Low Altitude Sattelites, *Phys. Scripta*, **75**, pp. 259-263, (1998)
- Boardsen, S.A., T.E. Eastman < T. Sofirelis, J.L. Green**, An empirical model of the high-latitude magnetopause, *J. Geophys. Res.*, **105**, 23193, (2000)
- Chandler, M. O., S. A. Fuselier, M. Lockwood, and T. E. Moore**, Evidence of component merging equatorward of the cusp, *J. Geophys. Res.*, **104**, 22,623, (1999).
- Chen, S.-H., S. A. Boardsen, S. F. Fung, J. L. Green, R. L. Kessel, L. C. Tan, T. E. Eastman, and J. D. Craven**, Exterior and interior polar cusps: Observations from Hawkeye, *J. Geophys. Res.*, **102**(A6), p. 11335, (1997)
- Chen, Q., A. Otto, L. C. Lee**, Tearing instability, Kelvin-Helmholtz Instability and Magnetic Reconnection, *J. Geophys. Res.*, **102** (A1), p. 151, (1997)
- Consolini, G. and A. T. Lui**, Symmetry breaking and nonlinear wave-wave interaction in current disruption: possible evidence for a phase transition, in *Magnetospheric Current Systems*, Geophysical Monograph **118**, American Geophysical Union, Washington D.C., pp. 395-401, (2000)

**Dubinín, E., A. Skalsky, P. Song, S. Savin, J. Kozyra, T. E. Moore, C. T. Russell, M. O. Chandler, A. Fedorov, L. Avánov, J. A. Sauvaud, R. H. W. Friedel,** Polar-Interball coordinated observations of plasma characteristics in the region of the northern and southern distant cusps, *J. Geophys. Res.*, **107**, A5, 10.1029/2001JA900068, (2002)

**Dungey, J. W.,** The structure of the exosphere, or adventure in velocity space in Geophysics the Earth's Environment, edited by C. DeWitt, J. Hieblot and A. Lebeau p.505, *Gordon and Breach*, New York, (1963)

**Fedorov , A., E. Budnik, J.A. Sauvaud,** On the origin of the high-latitude boundary layer, *Adv. Space Res.*, **30**, No. 12, 2763-2770, (2002)

**Fedorov , A., E. Dubinín, P. Song, E. Budnick, P. Larson, J.A. Sauvaud,** Characteristics of the exterior cusp for steady southward IMF: Interball observations, *J. Geophys. Res.*, **105**, 15,945- 15,957, (2000).

**Fung, S. F., T. E. Eastman, S. A. Boardsen and S.-H. Chen,** High-altitude cusp positions sampled by the Hawkeye satellite, *Phys. Chem. Earth*, **22**, pp. 653-662 (1997)

**Grande, M., J. Fennell, S. Livi, et al,** Observations of the mid-Altitude Magnetosheath During a Persistent Northward IMF Condition: Polar CAMMICE Observations, *Geophys. Res. Lett.*, **24**, pp. 1475-1478 (1997)

**Gustafsson, G., M. André, T. Carozzi, A. I. Eriksson, C-G. Fälthammar et al.,** FIRST RESULTS OF ELECTRIC FIELD AND DENSITY OBSERVATIONS BY CLUSTER EFW BASED ON INITIAL MONTHS OF OPERATION, *Annals Geophys.*, **19**, 1219- 1240, 2001.

**Haerendel, G. and G. Paschmann,** Entry of solar wind plasma into the magnetosphere, in *Physics of the Hot Plasma in the Magnetosphere*, edited by B. Hultqvist and L. Stenflo, p. 23, Plenum, NY, (1975)

**Haerendel, G.,** Microscopic plasma processes related to reconnection, *J. Atmos. Terr. Phys.*, **40**, pp. 343-353 (1978)

**Haerendel, G., et al.,** The frontside boundary layer of the magnetopause and the problem of reconnection, *J. Geophys. Res.*, **83**, 3195, (1978)

**Johnson, J.R., C.Z. Cheng ,** Kinetic Alfvén waves and plasma transport at the magnetopause, *Geophys. Res. Lett.*, **24**, p. 1423 (1997)

**Khotyaintsev, Y., et al.,** Transient reconnection in the cusp during strongly negative IMF By, *J. Geophys. Res.*, **106**, submitted (2003)

**Kirpichev, I., A. Fedorov, A. Grigoryev, E. Budnick, E. Dubinín,** Quasi-trapping of the charged particles in the local minimum of magnetic field in exterior cusp, *Cosmic Res. (Russia)*, **37**, No. 6, p. 638-643, (1999).

**Klimov, S. I. et al. ,** Investigation of plasma waves by combined wave diagnostic device BUDWAR PROGNOZ-10-INTERCOSMOS, *Cosmic Research (Transl. from Russian)*, **24**, 177, (1986)

**Klimov, S. et al. ,** ASPI Experiment: Measurements of Fields and Waves Onboard the INTERBALL-1 Spacecraft, *Ann. Geophys.*, **15**, pp.514-527, (1997)

**Kuznetsova, M. M., and L. M. Zelenyi,** The theory of FTE: Stochastic percolation model, in *Physics of Magnetic Flux Ropes*, edited by C. T. Russell, E. R. Priest, L.C. Lee, pp.473-488, *American Geophysical Union* (1990)

**La Belle-Hamer, A.L., A. Otto, L.C. Lee,** Magnetic reconnection in the presence of sheared flow and density asymmetry: application to the Earth's magnetopause, *J. Geophys. Res.*, **100**, pp. 11,875- 11,889, (1995)

**Lavraud, B., M. W. Dunlop, T. D. Phan et al.,** Cluster observations of the exterior cusp and its surrounding boundaries under northward IMF, *Geophys. Res. Lett.*, **29**, No. 20, 1995, (2002)

**Lundin, R., J. Woch and M. Yamauchi,** The present understanding of the cusp, in Proceedings of the Cusp Workshop, European Space Agency, *Spec. Publ.*, ESA SP-330, pp.83-95, (1991).

**Maynard, N.C., S.Savin, G.A.Erickson, H.Kawano, Z.Nemecek et al., ,** Observation of the magnetospheric "sash" and its implications relative to solar-wind/magnetospheric coupling: A multisatellite event analysis, *J. Geophys. Res.*, **106**, 6097, (2001)

**Merka, J, J. Safrankova, Z. Nemecek, A. Fedorov, N. Borodkova, S. Savin, A. Skalsky,** HIGH ALTITUDE CUSP: INTERBALL OBSERVATIONS, *Adv. Space Res.*, **25**, No. 7/8, pp. 1425-1434, (2000)

**Onsager, T.G., J. Scudder, M. Lockwood, C.T. Russell,** Reconnection at the high latitude magnetopause during northward IMF conditions, *J. Geophys. Res.*, (2001)

**Paschmann, G., G. Haerendel, N. Schopke, H. Rosenbauer and P. C. Hedgecock ,** Plasma and magnetic field characteristics of the distant polar cusp near local noon: The entry layer, *J. Geophys. Res.*, **81**, 2883, (1976)

**Petrinec, S. M. and C. T. Russell,** An examination of the effect of dipole tilt angle and cusp regions on the shape of the dayside magnetopause, *J. Geophys. Res.*, **100**, pp. 9559-9566, (1995)

**Pickett, J.S., J.D. Menietti, G.B. Hospodarsky, D.A. Gurnett, K. Stasiewicz,** *Adv. Space Res.*, **30**, No. 12, 2809-2814, (2002)

**Pilipenko, V., E. Fedorov, N. Mazur, M.J. Engebretson, W.J. Hughes ,** Magnetohydrodynamic waveguide/resonator for Pc3 ULF pulsations at cusp latitudes, *Earth Planets Space*, **51**, pp. 441-448 (1999)

**Popielawska, B., I. Sandahl, V. Styzhkin, H. Stenuit, A. Zakharov,** Magnetopause poleward of the cusp: comparison of plasma and magnetic signature of the boundary for southward and northward directed interplanetary magnetic field, *Adv. Space Res.*, **30**, No. 12, 2799-2808, (2002)

**Pottelle, R., M., Malingre, N., Dulouloz, B., Aparicio, et al.,** High frequency waves in the cusp/cleft regions, in *J. Geophys. Res.*, **95**, 5957, (1990)

**Romanov, S. A., S. I. Klimov, P. A. Mironenko,** Experimental Derivation of ELF .Wave Dispersion Relations and Evidence of Wave Coupling in the Earth Bow Shock Foot from the Data of the PROGNOZ-10, *Adv. Space Res.* **11**, 19 (1991)

- Romanov, S. A.**, A Correlation Analysis of Vector Variables as Applied to the Study of ELF Interplanetary Plasma Waves, *Cosmic Research*, **36**, No. 4, pp. 339-354 (1998)
- Romanov, V., S.Savin, S.Klimov, S.Romanov, Yu.Yermolaev, J.Blecki, R.Wronowski**, Magnetic turbulence at the magnetopause: plasma penetration, *J. Tech. Phys. (Poland)*, **40**, 1, 329-332, (1999).
- Russell, C. T.**, The configuration of the magnetosphere, in *Critical Problems of Magnetospheric Physics*, edited by E. R. Dyer, 1-16, *IUCSTP Secretariat*, Washington, D.C., (1972)
- Russell, C. T.**, The structure of the magnetopause, in *Physics of the Magnetopause*, edited by P. Song, B. U. O. Sonnerup and M. F. Thomsen, pp.81-98, *American Geophysical Union* (1995)
- Russell, C. T., *et al.*, The GGS Polar magnetic fields investigation, *Space Sci. Res.*, **21**, pp. 563-582, (1995)
- Safrankova, J., Z. Nemecek, D. Sibeck, L. Prech, J. Merka, O. Santolik**, Two-point observation of high-latitude reconnection, *Geophys Res. Lett.*, **25**, pp. 4301-4304, (1998)
- Sandahl, I.** Recent Cusp and Cleft Results from Interball, *Adv. Space Res.*, **30**, No. 7, 1711-1723, (2002)
- Savin, S. P.**, ELF waves near the high latitude magnetopause, in *Abstracts of AGU Chapman Conference on Physics of the Magnetopause*, March 14-18, 41, (1994)
- Savin, S. P., O. Balan, N. Borodkova, E. Budnik, N. Nikolaeva, V. Prokhorenko, T. Pulkkinen, et al.**, Interball Magnetotail Boundary Case Studies, *Adv. Space Res.*, **19**, 993, (1997)
- Savin, S. P., S. A. Romanov, A. O. Fedorov, L. Zelenyi, S. I. Klimov, et al.**, The cusp/magnetosheath interface on May 29, 1996: Integball-1 and Polar observations, *Geoph. Res.Lett.*, **25**, pp. 2963-2966, (1998a)
- Savin, S. P., N. L. Borodkova, E. Yu. Budnik, A. O. Fedorov, S. I. Klimov, et al.**, Interball tail probe measurements in outer cusp and boundary layers, in *Geospace Mass and Energy Flow: Results from the International Solar-Terrestrial Physics Program*, edited by J.L. Horwitz, D.L. Gallagher and W.K. Peterson, Geophysical Monograph **104**, American Geophysical Union, Washington D.C., pp. 25-44, (1998b)
- Savin, S., L. Zelenyi, L. Budnik, N. Borodkova, A. Fedorov, et al.** Manifestations of Boundary Layer Dynamics in Substorm Activity. Multi Spacecraft Study, in *SUBSTORM-4, International Conference on Substorms-4', Lake Hamana, Japan: March 9-13, 1998*, ed. by S. Kokubun and Y. Kamide, pp. 125-130, Terra Scientific Publ. Co., Tokyo, (1998c)
- Savin, S., E. Budnik, M. Nozdrachev, V. Romanov et al.**, On the plasma turbulence ant at the polar cusp outer border, *Chekhoslovak J. Phys.*, **49**, 4a, 679-693, (1999)
- Savin S.P., L.M. Zelenyi, S.A. Romanov, S.I. Klimov, A.A. Skalsky et al.**, Tubulent Boundary layer at the Border of Geomagnetic Trap, *JETP Letters*, **74**, No 11, pp. 547- 551, (2001)
- Savin, S., L. Zelenyi, N. Maynard, I. Sandahl, H. Kawano, C. T. Russell et al.**, Multi-spacecraft Tracing of Turbulent Boundary Layer, *Adv. Space Res.*, **30**, No. 12, 2821-2830, (2002a)
- Savin S., J. Buechner, G. Consolini, B. Nikutowski, L. Zelenyi, E. Amata, et al.**, On the properties of turbulent boundary layer over polar cusps, *Nonlinear Processes in Geophysics*, **9**, 443-451, (2002b)
- Savin, S., J. Blecki, N. Pissarenko, V. Lutsenko, I. Kirpichev, et al.**, ACCELERATED PARTICLES FROM TURBULENT BOUNDARY LAYER, *Adv. Space Res.*, **30**, No. 7, 1723-1730, (2002c)
- S. Savin, L. Zelenyi, S. Romanov, I. Sandahl, J. Pickett, E. Amata et al.**, Magnetosheath - Cusp Interface, *Ann. Geophys.*, (in press), (2003a)
- S. Savin, P. Song, A. Skalsky, L. Zelenyi, E. Amata et al.**, Interball-1 statistics for 'plasma balls' in outer cusp, *Geophys. Res. Lett.*, (submitted), (2003b)
- Smith, M. F., and M. Lockwood**, Earth's magnetospheric cusps, *Rev. of Geophys.*, **34**, 233,(1996)
- Song, P.**, Slow mode transition in the magnetosheath, *J. Geophys. Res.*, **97**, 8295 (1992)
- Spreiter, J. R., S. S. Stahara**, A new predictive model for determining solar wind- terrestrial planet interactions, *J. Geophys. Res.*, **85**, pp. 6769-6777, (1980)
- Spreiter, J. R., B. R. Briggs**, Theoretical determination of the form of the boundary of the solar corpuscular stream produced by interaction with the magnetic dipole field of the Earth, *J. Geophys. Res.*, **67**, pp. 37-51, (1962)
- Stasiewicz, K., C. E. Seyler,, G. Gustafsson,, J. Pickett and B. Popielawska**, Magnetic Bubbles and Kinetic Alfvén Waves in the High-Latitude Magnetopause Boundary; *J. Geophys. Res.*, **106**, 29503 (2001)
- Treumann, R.A., J. Labelle, T.M. Bauer**, Diffusion processes: an observational perspective, in *Physics of the magnetopause*, ed. by P. Song, B.U.O. Sonnerup, M. F. Thomsen, p. 331, American Geophysical Union (1995).
- Yamauchi, M., and R. Lundin**, The Wave-Assisted Cusp Model: Comparison to Low-Latitude Observations, *Phys. Chem. Earth*, **22**, pp. 729-734, (1997)
- Zelenyi, L.M., A.V. Milovanov**, Multiscale magnetic structure of the distant tail: self-consistent fractal approach, in *New Perspectives on the Earth Magnetotail*, Geophysical Monograph **105**, AGU, Washington D.C., pp. 321-338, (1998)
- Zelenyi, L. M., D. C. Delcourt, . V. Malova, A. S. Sharma, V. Yu. Popov, A. A. Bykov**, Forced Current Sheets in the Earth's Magnetotail: Their Role and Evolution due to Nonadiabatic Particle Scattering, *Adv. Space Res.*, **30**, No. 7, 1629-1638, (2002)
- Zhou, X.-W. and C. T. Russell**, The location of the high latitude polar cusp and the shape of the surrounding magnetopause, *J. Geophys. Res.*, **102**, pp. 105-110, (1997)